Karlsruhe Institute of Technology

Using a Building as Thermal Storage and Model Predictive Control of a Heat Pump for Grid Stabilization

Master's thesis of

Vivien Geenen

at the Department of Mechanical Engineering
Institute for Automation and Applied Informatics (IAI)

Reviewer:	Prof. Dr. Veit Hagenmeyer
Second reviewer:	apl. Prof. Dr. Jörg Matthes
Advisor:	Moritz Frahm, M.Sc. and Frederik Zahn, M.Sc.

14. June – 14. December 2021

I declare that I have developed and written the enclosed thesis completely by myself, and have not used sources or means without declaration in the text.

PLACE, DATE

. . . . . .

(Vivien Geenen)

Kurzfassung

Abstract

Contents

Kurzfassung i

Abstract ii

1 Introduction 1

1.1 Objective of this work . . . 2
1.2 Related work . . . 2
1.3 Content structuring . . . 4

2 Foundations 5

2.1 Thermal basics . . . 5
2.1.1 Balancing energy . . . 5
2.1.2 Conduction . . . 6
2.1.3 Convection . . . 7
2.1.4 Radiation . . . 7
2.2 Lumped capacitance model . . . 8
2.2.1 Electrical analogy . . . 8
2.3 Model predictive control (MPC) . . . 10
2.3.1 Cost function . . . 12
2.3.2 Dynamics . . . 12
2.3.3 Constraints . . . 13
2.4 The reference building . . . 13

3 Modelling 15

3.1 The modelling strategies . . . 15
3.2 The water reservoir model . . . 17
3.3 The building model . . . 18

3.3.1 Parameter identification . . . 21
3.3.2 Training and verification of the thermal model . . . 22
3.4 The state-space formulation . . . 24

4 Experiments **26**
4.1 Experiment 1 . . . 26
4.1.1 Data of the experiment 1 . . . 27
4.2 Experiment 2 . . . 28
4.2.1 Data of the experiment 2 . . . 29
4.3 Findings of the experiments . . . 30

5 Model predictive control **32**
5.1 Framework conditions of the MPC . . . 32
5.1.1 Characteristic diagram of the heat pump . . . 32
5.1.2 Occupancy schedule . . . 33
5.1.3 Used data . . . 34
5.2 The Constraints . . . 35
5.2.1 Constraints of the control signals . . . 35
5.2.2 Constraint of the output . . . 36
5.2.3 Constraints of the states . . . 36
5.2.4 Integration method and its constraint . . . 37
5.3 The Cost function . . . 38
5.4 Workflow of the MPC script . . . 39
5.5 Choice of weightings and horizon . . . 40
5.5.1 Average comfort and grid services over the weightings . . . 41
5.5.2 Choice of the horizon . . . 42

6 Results and discussion **45**
6.1 Results of the scenarios . . . 45
6.1.1 Presentation of the scenarios . . . 45
6.1.2 Results of the scenarios . . . 46
6.2 Discussion . . . 51
6.2.1 Comparison of the scenarios . . . 52
6.2.2 General discussion about the approach . . . 54

7 Conclusion **55**

8 Outlook **56**

Bibliography **57**

A Appendix **64**

A.1 Model values 64
A.2 Matrices of state-space formulation 64
A.3 Laboratory journal 67
A.4 Average comfort and grid services 69

List of Figures

2.1 Sample of a wall with thermal resistances 9
2.2 Sample RC- network 9
2.3 MPC structure of the control loop 11
2.4 Construction plan of the building [37] 14

3.1 Illustration of the water reservoir with the heat flows 17
3.2 Structure of the thermal model in RC- analogy 21
3.3 Workflow of grey-box modelling with Matlab 21
3.4 Training of the building model 23
3.5 Verification of the building model 24
3.6 RMSE and R_{max} of the output for training and verification period 24

4.1 Electrical consumption of the building and air temperature inside the rooms during the experiment 1 28
4.2 Electrical consumption of the building and air temperature inside the rooms during the experiment 2 30

5.1 Interpolation of the characteristic diagram of the heat pump with nominal power according to [40] 33

5.2 Occupancy schedule of the reference building 34
5.3 Dynamic price of electricity [53] and shifted dynamic price of electricity . . 35
5.4 Workflow of the MPC script 40
5.5 $\Delta\overline{y}$ and GS for N = 24h 42
5.6 Measured data of the reference building: T_{inside} over three days 43
5.7 Curve of the sum of cost over simulation time for different N 44

6.1 T_{inside} for the three scenarios for $i_1 = 0.1 and i_2 = 0.9$ and $i_1 = 0.9 and i_2 = 0.1$. 47
6.2 $\dot{Q}_{\text{heating}}$ for the three scenarios for $i_1 = 0.1 and i_2 = 0.9$ and $i_1 = 0.9 and i_2 = 0.1$ 48
6.3 $\dot{Q}_{\text{HP}}$ for the three scenarios for $i_1 = 0.1 and i_2 = 0.9$ and $i_1 = 0.9 and i_2 = 0.1$ . . 49
6.4 P_{HP} and Pr for the three scenarios for $i_1 = 0.1 and i_2 = 0.9$ and $i_1 = 0.9 and i_2 = 0.1$ 50

A.1 AC and GS for N = 12h 69
A.2 AC and GS for N = 18h 69
A.3 AC and GS for N = 30h 70

List of Tables

2.1 dimensions of the matrices 12

3.1 Advantages and disadvantages of grey-box modelling 16
3.2 Advantages and disadvantages of white-box modelling 16
3.3 Explanation of the special material and state dependant values of the differential equation of the inside temperature 19
3.4 Explanation of the special material and state dependant values of the differential equation of the envelope temperature 20
3.5 Conclusion of relevant information about the grey-box model 23

4.1 Technical data and configuration during the experiments [50], [51], [52] . . 27

5.1 Weighting factor 39
5.2 $\Delta\overline{y}$ for different N 42
5.3 GS for different N 42

6.1 $\Delta\overline{y}$ of the scenarios according to i_1 51
6.2 GS of the scenarios according to i_2 51
6.3 Energy consumption of the scenarios according to the weighting 51

A.1 Start and identified values of the model parameters 64
A.2 Laboratory journal: 16. July - 18. July 2021 67
A.3 Laboratory journal: 26. July - 1. August 2021 68

1. Introduction

Climate change is challenging the entire world. In the Paris Agreement, the United Nations (UN) agrees to keep the rise in global average temperature significant under two degrees Celsius [1]. To achieve this aim every nation has to reduce its greenhouse gas emissions. This calls for changes in the mobility sector, industry, and energy production, for example. The German government intends to implement this by promoting electromobility, using hydrogen in industry, and energy transition [2]. In particular, the so-called energy transition that has already been initiated has to be driven forward. That means the expansion of renewable energies and decreasing conventional power plants. The German government is aiming to phase out coal-fired power plants by 2038 [3]. For covering the energy demand, a high increase in energy from renewable sources, e.g. photovoltaics and wind power, is necessary for the coming years.

Unfortunately, a disadvantage of these renewable energy sources is that they fluctuate with the weather and cannot produce energy on demand. In addition, more renewable energy sources can lead to more intense imbalances in the grid. To compensate the imbalances in the grid, the grid requires or releases energy. In order to have enough energy available, the amount of storage options must grow with the amount of renewable energy sources. Batteries, pumped hydroelectric energy storage, thermal energy storage, and many other technologies could store an excess of power during a sunny or windy day. Furthermore, the necessity of demand side management (DSM) rice also with the increasing renewable energy sources, then DSM can shift loads to balance the grid. Load shifting is part of DSM [4] and already used in the industry. Another approach is to use residential buildings as thermal storage and demand response to contribute to grid balance[5]. As a promising DSM technology, the control of heating, ventilation, and air conditioning (HVAC) systems could be used. Particularly controlling heat pumps of buildings seem auspicious. As at least 1.25 million heat pumps are already installed in Germany, and their number is increasing steadily [6].

The implementation of this approach needs a control strategy ensuring consumer comfort

also during changing weather conditions. Model predictive control (MPC) is a suitable tool to integrate forecasts of weather and control heat pumps in buildings for stabilizing the grid with the thermal storage of the building. Research has already shown the possibilities of MPC to shift loads, to save energy and costs [7], [8], [9]. On the other hand, researchers investigate the impact of occupancy plans on energy consumption in buildings. They prove a significant energy-saving potential [10]. This thesis picks up the advantages of an occupancy plan, and it analyses consumption, comfort, and grid service of an MPC with and without an occupancy plan of the building.

1.1. Objective of this work

This thesis aims to design a control system, which simultaneously serves the grid and comply with the required comfortable internal temperature range, for the heat pump of a building in the so-called "Living Lab" of the Karlsruhe Institute of Technology (KIT) at Campus North. The implementation is to be carried out using the control method Model Predictive Control. This method enables to predict the future thermal behaviour of the building and to react to the current and future fluctuations of the weather or the grid for example. In the first step, a thermal model of the building behaviour must be created. For this purpose, the physical structure of the model is to be determined. Appropriate assumptions can be made to reduce the complexity of the thermal behaviour of the building.Furthermore, the parameters of the model are determined by a parameter identification from measurements to obtain a grey-box model, i.e., a combination of physical model structure and optimisation with measurement data. After the verification of the thermal model using measured data from the Energy Lab 2.0 from the KIT, an optimal control problem shall be created. The aim is to construct an MPC algorithm and to simulate its application. The software used will be Matlab/Simulink.

1.2. Related work

Extant literature investigates thermal modelling and controlling of buildings. Kramer et al. [11] summarize in a literature review thermal modelling approaches such as white-box, grey-box, and black-box models and present how researchers apply these approaches. Further authors identify their thermal model parameters with measurements and use the grey-box modelling approach [12], [13], [14]. Coakley et al. [15] see the advantages of grey-box mod-

elling in the short development time for the model, fidelity of predictions, and the interaction of building, system and environmental parameters. One disadvantage is that modellers need a high level of knowledge in physical and statistical modelling [15]. Furthermore, Cigler et al. [16] and Hazyuk et al. [8] see the advantages of grey-box models and work with them in their MPC applications for thermal management in buildings.
Regardless of the type of model, MPC is utilised for control of heating, ventilation, and air conditioning (HVAC) systems in buildings for a variety of reasons, e.g. [8], [9], [7]. Researchers are interested in the reduction of energy consumption [8] and saving costs [9] while obtaining thermal comfort. Oldewurtel et al. [7] present how to decrease or shift the peak load of buildings.
On the other hand, [17] and [5] refer to the potential of heat pumps for grid services. Among others, the report "Wärmepumpen in Bestandsgebäuden" examines the load shifting potential of grouped heat pumps. The researchers determine 4 to 14 GWh load shifting potential for one million heat pumps [17]. Kohlhepp and Hagenmeyer [5] introduce a method to assess the technical potential of HVAC systems for grid services. Especially, they detect for heat pumps 5.2 TWh electrical demand in Germany per year.
Avci et al. [18] apply MPC for heat pumps to the realization of grid services. They give an early indication of the potential of grid services using real-time pricing. For application of DSM, most researches apply a dynamic price signal, although their focus differs e.g. according to the type of buildings [19], [20] or the type of optimisation [19], [21].
Another interesting field of research is the energy saving potential by planing the occupancy of buildings. Wang et al. [10] show in their paper that 13 percent of energy can be saved by occupancy-based controls for an office building. Liang et al. [22] investigate an occupancy schedule with for example machine learning approaches to better control of HVAC systems and consequently to save energy.

This thesis integrates occupancy schedules into the MPC formulation to investigate the potential of included occupancy behaviour on control metrics. A simple occupancy plan is used to examine whether comfort, grid services, and energy consumption can be improved compared to an MPC without an occupancy plan. Consequently, in this thesis, an MPC is created with a grey-box model and grid services are implemented with real-time pricing, similar to the papers cited above. But in this thesis, the potential of an occupants schedule is analysed at a real reference building during focusing on the aim of grid services. This thesis

finds an answer to the question: How does the inclusion of an occupancy schedule in an MPC improve grid services, energy consumption and comfort?

1.3. Content structuring

Stukturierung meiner Thesis erläutern

2. Foundations

The issue of this thesis is to create a thermal model of a real building and to optimise the control signals that influence the thermal model. For thermal modelling, some basics about the energy balance and the heat flows are needed and therefore introduced in this chapter. In addition, the RC-analogy is used since the analogy simplifies the creation of a model and is also explained. For optimisation, the model predictive control (MPC) approach is described in detail. Finally, the features of interest of the real building are summarised.

2.1. Thermal basics

2.1.1. Balancing energy

It is necessary to comprehend the basics of thermodynamics to understand the structure of a thermal model. The first law of thermodynamics is the general energy balance and is formulated for unsteady and open systems as follows [23]:

$$\sum_i \dot{Q}_\mathrm{i} + \sum_j \dot{W}_\mathrm{j} + \sum_k \dot{m}_\mathrm{k} \cdot (h + \frac{c^2}{2} + gz)_\mathrm{k} = \frac{d}{dt} \sum_l U_\mathrm{l} \tag{2.1}$$

In terms of a building, we set the work $\dot{W}$ to zero according to the relationship $W = \int Pdt - \int pdV$ [23] because a building can't change the volume V, and we have no additional mechanical power P. If we have no mass flow $\dot{m}$ in our system, we obtain a closed system. Regarding buildings, mass flows could be airflow through the window, for example. Then we also consider the enthalpy h, the fluid velocity c, the high z and the gravitational acceleration g.
Since we do not consider airflow, we use the closed system with the heat flows $\dot{Q}_\mathrm{i}$ and the inner energy U_l.

$$\sum_i \dot{Q}_\mathrm{i} = \frac{d}{dt} \sum_l U_\mathrm{l} \tag{2.2}$$

The deduction of the inner energy U starts with the complete differential description of the specific inner energy du as [23]:

$$du = (\frac{\partial u}{\partial T})_{\mathrm{v}} dT + (\frac{\partial u}{\partial v})_{\mathrm{T}} dv \tag{2.3}$$

The specific volume dv is negligible in buildings, and the specific heat capacity during constant volume has the expression $c_{\mathrm{v}} = (\frac{\partial u}{\partial T})_{\mathrm{v}}$ [23]. After replacing the specific values by volume, we obtain the relation for the inner energy U, with the mass m.

$$dU = mc_{\mathrm{v}} dT \tag{2.4}$$

It applies to substances with a specific volume regardless of the pressure that $c_{\mathrm{v}} = c_{\mathrm{p}} = c$.

We account for different heat flows and for the inner energy in the energy balance in Equation 2.1. However, there are three mechanisms of heat transfer, which are explained in the following sections: Heat conduction, heat convection, and heat radiation [24]. Thermal modelling of buildings requires all of these mechanisms. For example, conduction is the primary part of heat transfer through walls or floors. Convection occurs on the inside and the outside of the building between the walls and the air. To integrated the impact of the sun, radiation is needed, for example.

2.1.2. Conduction

Conduction means that heat energy is directed in a solid or fluid. Molecules within the solid or fluid have higher energy when the temperature is higher. They transfer the energy to neighbouring molecules with smaller energy. Without a heat source, the temperature difference between a hot and a cold location of the molecules decreases.[25]
The equation

$$\dot{\mathbf{q}} = -\lambda \nabla T \tag{2.5}$$

describes the conduction according to Fourier [24]. λ is the thermal conductivity with the assumption of being constant and $\dot{\mathbf{q}}$ and T represent the specific heat flux and the temperature. The thermal conductivity is dependent on the material, such as concrete, wood or bricks.
To know the heat flux $\dot{Q}$, it is necessary to expand the above equation with the area A,

the thickness of the conductive medium d and a temperature difference ΔT assuming one significant direction of the heat flux $\dot{Q}$ to:

$$\dot{Q} = \frac{A\lambda}{d}\Delta T \tag{2.6}$$

In terms of buildings, the conductive medium could be walls, floors or roofs.

2.1.3. Convection

Macroscopic movements of a fluid lead to the transport of kinetic energy and enthalpy. This mechanism is called convection. These movements are generated by external forces or by internal forces like balancing the pressure or temperature [24].
Newton's law of cooling describes the convective heat transfer $\dot{Q}$ as

$$\dot{Q} = \alpha A(T_w - T_\infty) \tag{2.7}$$

with the heat transfer coefficient α , especially for building modelling the wall temperature T_w and the environment temperature T_∞ [26] . There are two possibilities to determine the heat transfer coefficient. Both require a temperature difference ΔT and either a temperature gradient $\partial T/\partial x$ or a heat flux $\dot{Q}$. [24]

2.1.4. Radiation

Every body emits heat radiation to the environment with electromagnetic waves. Heat radiation does not need matter for energy transportation. As shown in the following equation, the temperature T of the body influences heat radiation.[24]

$$\dot{q} = \sigma T^4 \tag{2.8}$$

This correlation applies to a black body, where $\dot{q}$ is a heat flux and σ represents the Stefan-Boltzmann coefficient. A black body absorbs all heat radiation with all wavelengths from all directions[26]. The consideration of a black body is idealized. For the illustration of a real body (see Equation 2.9), the emissivity ϵ is used. ϵ is material-dependent and lies between 0 and 1.

$$\dot{q} = \epsilon\sigma T^4 \tag{2.9}$$

In general, a body absorbs, transmits, and reflects radiation with the appropriate coefficients a, τ and r. The sum of three coefficients has to be one ($a + \tau + r = 1$) [27].
The primary source of heat radiation is the sun, which plays an important role in the thermal modelling of buildings. Objectives in the building, such as radiators, also radiate heat. For example, radiators have equal parts convective and radiative energy transport [28].

2.2. Lumped capacitance model

For modelling the thermal behaviour of buildings, the lumped capacitance model is often used. With this approach, using the electrical analogy, building elements are represented by resistors R and capacitors C [11].

2.2.1. Electrical analogy

Similar to an electrical network, the potential is represented by the temperature at one node and the heat flux corresponds to the current. In analogy to the electric domain, we can describe the Ohm's law in heat transfer by:

$$\dot{Q} = \frac{\Delta T}{R} \tag{2.10}$$

Combining the above equation with Equation 2.6 or Equation 2.7, the thermal resistance R is determined in conductive cases as [25]:

$$R_\lambda = \frac{d}{A\lambda} \tag{2.11}$$

and in convective cases as[26]:

$$R_\alpha = \frac{1}{\alpha A} \tag{2.12}$$

Thermal resistances can be summarised to one thermal resistance, even if they are from different mechanisms of heat transfer. Based on an example in Figure 2.1, the addition is explained. The figure shows a section of a wall with a heat flow $\dot{Q}$, the ambient temperature T_1 and T_2 separated by that wall. We have three thermal resistances $R_{\alpha,1}$, $R_{\alpha,2}$, and R_λ, which we sum to one thermal resistance $R = R_{\alpha,1} + R_\lambda + R_{\alpha,2}$. Now, we can calculate the heat flow $\dot{Q} = \frac{T_2 - T_1}{R}$ according to Equation 2.10.

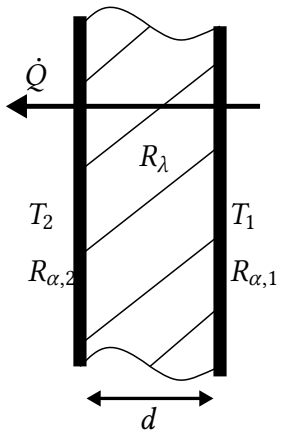

Figure 2.1. Sample of a wall with thermal resistances

In sum, the thermal resistances R comply with electrical resistors. Further for modelling thermal networks, the thermal capacitance C is needed. It is calculated from the specific heat capacity c multiplied by the mass m ($C = cm$).
For a better explanation of the structure of a thermal network, a simple example is depicted in Figure 2.2. It represents a heated wall of a building. The heat flux $\dot{Q}$, for example from a

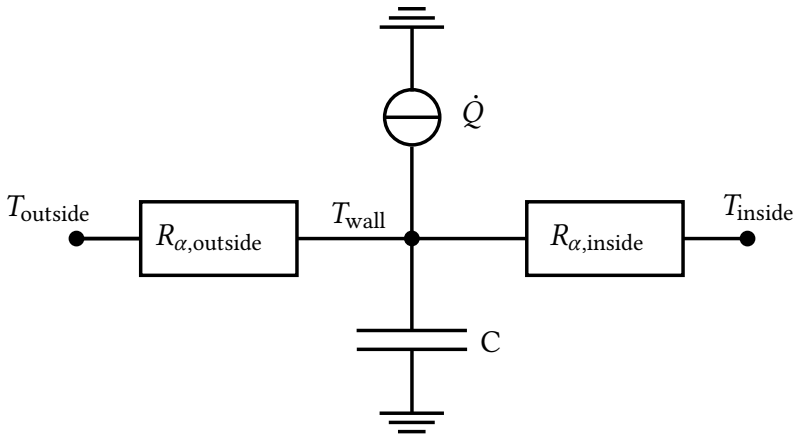

Figure 2.2. Sample RC- network

radiator, influences the temperature T_{wall}, as well as the capacitance C. And the temperature T_{wall} affects the temperature inside and outside T_{inside} and T_{outside} with their resistances $R_{\alpha,\text{inside}}$ and $R_{\alpha,\text{outside}}$. The example shows that all connections in the network influence each other. To

model the dynamics of the wall in differential equations, Kirchhoff's Current Law is required. It states that the sum of the flowing current to the node is equal to the sum of the flowing current of the node [25]. Because of the thermal analogy of electrical laws, the current is replaced by heat flux. The following differential equation results for the node T_{wall} using Ohm's law ($\dot{Q} = \Delta T/R$) and the first low of thermodynamics as deduced in Equation 2.2 with the inner energy from Equation 2.4.

$$C\frac{dT_{\text{wall}}}{dt} = \dot{Q} + \frac{T_{\text{inside}} - T_{\text{wall}}}{R_{\alpha,\text{inside}}} - \frac{T_{\text{wall}} - T_{\text{outside}}}{R_{\alpha,\text{outside}}} \tag{2.13}$$

In Figure 2.2, the thermal resistances are serially connected. According to the electrical network, resistances in series are equal to their sum.

$$R_{\text{sum}} = R_{\alpha,\text{inside}} + R_{\alpha,\text{outside}} \tag{2.14}$$

A parallel circuitry has windows and walls in buildings, for example. Here the resistances are calculated according to the following schema:

$$\frac{1}{R_{\text{sum}}} = \frac{1}{R_{\text{wall}}} + \frac{1}{R_{\text{window}}} \tag{2.15}$$

In terms of needed more capacitances for describing the thermal model, the summary capacitance is added in a parallel circuitry as:

$$C_{\text{sum}} = \sum_{1}^{i} C_{\text{i}} \tag{2.16}$$

The serial circuitry of capacitances is calculated as follows:

$$\frac{1}{C_{\text{sum}}} = \sum_{1}^{i} \frac{1}{C_i} \tag{2.17}$$

2.3. Model predictive control (MPC)

Model predictive control exploits models of the plant to predict and optimise the behaviour of the plant [29]. Applied to thermal control of a building with the aim of grid-supporting, a model of the thermal behaviour of the building is required to predict the reaction of the

system behaviour in the next N time steps, called the prediction horizon. Every time step k, the current state $\mathbf{x_k}$, the output $\mathbf{y_k}$ is measured, and the future system behaviour is obtained by computation. The computation of the future system behaviour may include measurable disturbances $\mathbf{d_k}$ such as weather forecast, occupancy schedule and the optimisation of the control signal $\mathbf{u_k}$ over the optimisation horizon $\mathbf{u_{k+N}}$. However, only the first calculated control signal is adopted as input for the plant. Then, the calculations are repeated at every time step. Figure 2.3 visualises the MPC control loop.

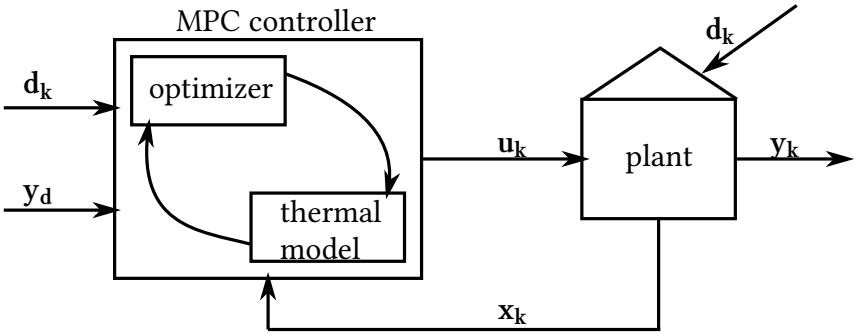

Figure 2.3. MPC structure of the control loop

Concluded, the MPC is "an iterative online optimisation over the predictions" [29] compiled by the thermal model of the building. Mathematically explained, the optimizer needs to minimize the following equation according to [30] and [31]:

$$\text{Cost function} \qquad \text{minimize} \sum_{k=1}^{N-1} c_k(\mathbf{x_k}, \mathbf{u_k}, \mathbf{y_k}) \tag{2.18}$$

subject to

$$\begin{aligned}
\text{Current state} \quad & \mathbf{x_0} = && \mathbf{x} \\
\text{Dynamics} \quad & \mathbf{x_{k+1}} = && f(\mathbf{x_k}, \mathbf{u_k}, \mathbf{d_k}), \qquad \mathbf{y_k} = g(\mathbf{x_k}, \mathbf{u_k}, \mathbf{d_k}) \\
\text{Constraints} \quad & \mathbf{y_{min}} \leq && \mathbf{y_k} \leq \mathbf{y_{max}} \\
& \mathbf{u_{min}} \leq && \mathbf{u_k} \leq \mathbf{u_{max}}
\end{aligned}$$

c_k represents the cost function, which is explained in detail in subsection 2.3.1 . In terms of building control, y is the internal temperature.

	m	n
A	number of states	number of states
B_1	number of states	number of control signals
B_2	number of states	number of disturbances
C	number of outputs	number of states
D_1	number of outputs	number of control signals
D_2	number of outputs	number of disturbances

Table 2.1. dimensions of the matrices

2.3.1. Cost function

Generally, the cost function c_k assigns a cost to the control signal $\mathbf{u_k}$ and the current state $\mathbf{x_k}$, which is mathematically described in Equation 2.18 , with:

$$c_k = (\mathbf{x_k^T} Q \mathbf{x_k} + \mathbf{u_k^T} R \mathbf{u_k}) \tag{2.19}$$

Here Q and R are matrices over which individual elements of the state vector or control signal vector can be weighted differently. [32] Especially for every application, the cost function has an individual form to reach the aims of the MPC.

2.3.2. Dynamics

The state-space formulation (SSF) is an alternative representation of a linear differential equation, which models a physical system. In this work, it is used for the formulation of the thermal model, which is required for the MPC. The SSF consists of the state $\mathbf{x}$, the control signal $\mathbf{u}$, the disturbances $\mathbf{d}$ and the output of the system $\mathbf{y}$ are represented in Equation 2.20. The system matrix is A, B_1 and B_2 are called the input matrices, C is the output matrix, D_1 and D_2 are the pass-through matrices. The Table 2.1 lists the dimensions of the matrices m x n with m rows and n columns.

$$\begin{aligned} \dot{\mathbf{x}} &= A\mathbf{x} + B_1\mathbf{u} + B_2\mathbf{d} \\ \mathbf{y} &= C\mathbf{x} + D_1\mathbf{u} + D_2\mathbf{d} \end{aligned} \tag{2.20}$$

Every differential equation needs initial values for solving. Therefore, initial states $\mathbf{x_0}$, initial control signals $\mathbf{u_0}$, and initial disturbances $\mathbf{d_0}$ must be given. In a thermal model of a building, some authors ([28], [33]) use the state as a vector of some temperatures, the control

signal as a signal for the heating system, the disturbances can describe the influence by the weather or occupants and the output of the system contains frequently the temperature inside of the building.

2.3.3. Constraints

Dealing with constraints is one of the most important advantages of MPC. Thereby, constraints can be used for the state, the output, and the input. In terms of building control, output constraints and input constraints are reasonable, as mathematically described in the Equation 2.18. That means, the output constraints could be a temperature range, which feels comfortable for occupants. And the constraints for the input are given as minimal (= 0) and maximal values of the possible performances. General, logical and physical ranges are constrained. There are different forms of constraints, but linear constraints are frequently used for MPC because they simplify the optimisation problem. Constraints can also be time dependant. This is beneficial for embedding diverse temperature ranges during the night and the day or during the working time of occupants when they are not at home. [33]

2.4. The reference building

Since this thesis is based on a real building, the necessary details about the building will be described below. The building is located on the "Campus Nord" of the KIT and is part of the "Energy Lab 2.0", "a research infrastructure for renewable energy"[34]. It is equipped with a kitchen, a bathroom, five rooms and a technical room. For a better orientation, Figure 2.4 shows a part of the construction plan of the building. The building is designed as a single-family house, but for practical reasons, it is used as an office. The living area is around 100 m^2. The building offers two options to heat or cool with a ground-source heat pump or an air heat pump. The focus is on the air heat pump because the most commonly used heat pumps in Germany are air heat pumps [35]. In addition to the heat pump, there is a water reservoir for saving energy with stratified storage. The total volume is 1000 litres [36]. The heating system inside the building is provided as underground floor heating. However, the heating system is not completely installed yet. So using the heat pump, the water reservoir or the underground floor heating is not possible, yet.
One of the main features of the building is the number of sensors. The air temperature is measured in every room, as well as the temperature in the middle of the exterior walls,

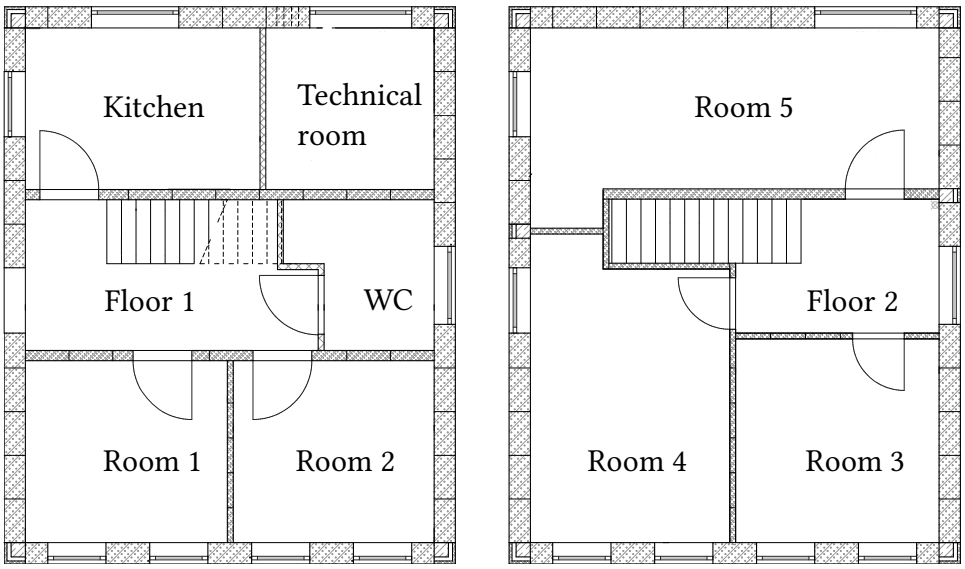

Figure 2.4. Construction plan of the building [37]

the screed temperature, the floor plate temperature, and the temperature of the inner wall between room three and room four (see Figure 2.4). Furthermore, the consumption of the actual electrical power is also detected. Only the mentioned sensors are needed in this case, but there are many more sensors.

3. Modelling

After explaining thermal basics and the electrical analogy, these foundations are used in this chapter. The development process and the results of the thermal model of the reference building will be presented. Later, the model is needed for the MPC to predict the thermal reactions of the building.

The focus of this work is on the MPC part, so a simple thermal model is required. Nevertheless, no necessary information should be missing: (i) the thermal storage possibilities, (ii) the temperature inside of the building, and (iii) the influence of the heating system. The storage allows heating while the grid has too much power and saving energy in the building, while the grid requires power. This behaviour is necessary to achieve the MPC's goal of providing grid services. The output of the model must be the inside temperature, as customer comfort is controlled by the air temperature using the MPC. Finally, the influence of the heating system must be visible in the model, as it is the input of the system.
The thermal model reflects the thermal conditions of the reference building. Therefore, the inner energy of the water reservoir and the air temperature inside the building are modelled. The water reservoir and the building behaviour are modelled according to different modelling strategies. The following chapters describe the submodels water reservoir and building model, the kind of modelling, and the conclusion of the submodels.

3.1. The modelling strategies

There are three types of modelling strategies to derive building models the so-called white-box models, grey-box models or black-box models. White-box models describe the system in terms of first principles from physics. Black-box models, on the other hand, have no physical description. They are created from data. And grey-box models are in between these two options [38]. All approaches are used in the thermal modelling of buildings [11].

The chosen approach for the MPC is the **grey-box model** for two reasons: First, this approach combines the advantages of white-box models and black-box models [39]. Second, there is the possibility to generate the required data from the reference building with the available measurement equipment at KIT. According to Coakley et al., further advantages and disadvantages are among other things [15]:

Advantages	Disadvantages
• faster development by a combination of physical and statistical model	• requires knowledge in physical and statistical modelling
• accuracy of the results for the specific use case, provided by qualitative training data	• changes at the building lead to a retraining

Table 3.1. Advantages and disadvantages of grey-box modelling

However, the water reservoir and the heating system are not in use, yet. So, no data is available for training a grey-box model. Thus, this submodel needs to be designed as a **white-box model**.
The benefits and challenges of white-box models are presented in Table 3.2 [39].

Advantages	Disadvantages
• relies on physics	• necessitate assumptions for simplification
• applicable for every situation with the same assumptions and requirements	• commonly complex mathematical solution methods

Table 3.2. Advantages and disadvantages of white-box modelling

3.2. The water reservoir model

For the modelling of the water reservoir (WR) , all heat flows that influence the water reservoir are considered (see Figure 3.1). The heat pump (HP) feeds the water reservoir with heat flow $\dot{Q}_{\mathrm{HP}}$. The service water (SW) and the water for the heating circuit are removed from the storage. Since no service water is currently connected to the reference building, the heat flow $\dot{Q}_{\mathrm{SW}}$ will be set to zero in the following. The heat losses $\dot{Q}_{\mathrm{loss}}$ and the heating heat flow $\dot{Q}_{\mathrm{heating}}$ are the discharged heat flows. The resulting energy balance according to Equation 2.1 reads:

$$\frac{dU_{\mathrm{WR}}}{dt} = -\dot{Q}_{\mathrm{heating}} + \dot{Q}_{\mathrm{HP}} - \dot{Q}_{\mathrm{loss}} \tag{3.1}$$

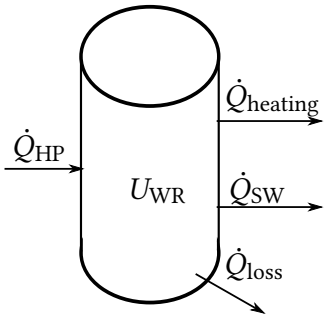

Figure 3.1. Illustration of the water reservoir with the heat flows

Since the model is based on a real building, the size of the heat flows and the inner energy are limited according to the devices of the building, e.g. the heat pump. Further, we have to consider that the heat flows $\dot{Q}_{\mathrm{HP}}$ and $\dot{Q}_{\mathrm{heating}}$ can also have negative values when cooling is required. The heat losses and the heat pump heat range are taken from the technical data [36], [40].

Since the reference water reservoir is stratified storage we determine the maximum inner energy under the assumption of two heat layers. According to Equation 2.4, we need material parameters of water ($c_{\mathrm{v,w}}$, ρ_{w}), the size of the water reservoir ($m = \rho_{\mathrm{w}} V$), both are known, and a temperature difference, which we define for both layers. To determine the temperature difference, we define two temperatures at the time one and two. At the time one, we assume that the storage has ambient temperature T_{amb} of 20°C in both layers. At the time two, we differentiate the temperatures in the layers. The maximum temperature of the upper layer in the water reservoir $T_{\mathrm{max,1}}$ is the maximum inlet temperature of 55 °C of the heat pump provided by the characteristic diagram. The maximum temperature of the lower layer $T_{\mathrm{max,2}}$

is based on the inlet temperature of the underfloor heating at 35 °C. We calculate the sum of the inner energy as follows.

$$U = \rho_{\mathrm{w}} c_{\mathrm{v,w}} ((T_{\mathrm{max},1} - T_{\mathrm{amb}}) \cdot \frac{V}{2} + (T_{\mathrm{max},2} - T_{\mathrm{amb}}) \cdot \frac{V}{2}) \tag{3.2}$$

3.3. The building model

First, the thermal dynamics of the building must be described physically. To comply with the requirement of a simple model, we model the building as a single zone, as often practised in the literature [41], [28]. Single zone means that we average the values of interest of the rooms, such as air temperature or wall temperature to one representative value for the entire building.
We consider the air temperature, the temperature of the outer walls, the temperature of the inner walls and floors in the first floor, and the temperature of the floor in the model. In the following, these temperatures are called: inside temperature T_{inside}, envelope temperature T_{envelope}, interior temperature T_{interior}, and floor temperature T_{floor}. Using the state-space formulation (see subsection 2.3.2), the temperatures are states in this model. According to the RC-analogy (see subsection 2.2.1), the model is built and explained in more detail in the following for every state.

Inside temperature:
The inside temperature T_{inside} is the main parameter in the model because we control it in the MPC. To generate high accuracy the impacts on T_{inside} are modelled more specific. Therefore, compared to the description of the other states, a more precise description of the dynamics of the inside temperature is required. We consider the influence of the sun $\dot{Q}_{\mathrm{sun,inside}}$, the heating system $\dot{Q}_{\mathrm{heating}}$ and the other states in the way shown in the following equation. $\dot{Q}_{\mathrm{heating}}$ links the water reservoir model and the building model as the flow from the reservoir to the building.

$$\begin{aligned} C_{\mathrm{inside}} \cdot \frac{dT_{\mathrm{inside}}}{dt} = \quad & \dot{Q}_{\mathrm{heating}} + \dot{Q}_{\mathrm{sun,inside}} - \frac{T_{\mathrm{inside}} - T_{\mathrm{envelope}}}{R_{\mathrm{inside}}} - \frac{T_{\mathrm{inside}} - T_{\mathrm{outside}}}{R_{\mathrm{window}}} \\ & - \frac{T_{\mathrm{inside}} - T_{\mathrm{interior}}}{R_{\mathrm{interior}}} - \frac{T_{\mathrm{inside}} - T_{\mathrm{floor}}}{R_{\mathrm{floor}}} \end{aligned} \tag{3.3}$$

The detailed explanation for the composition of the thermal resistance and capacitance is in subsection 2.2.1. In the following table, the material and state dependant values are explained:

C_{inside}	The thermal capacitance C_{inside} is calculated from the mass of the air from all rooms and the heat capacity of the air (1006 $J/(kgK)$ [42]). The mass can be determined with the volume of the rooms according to the construction plan [37] and the air density (1.28 kg/m^3 [42]).
R_{inside}	The thermal resistance R_{inside} includes a convective part with the transfer coefficient $\alpha = 0.9W/(m^2K)$ for air perpendicular to the wall in buildings with the assumption of one Kelvin temperature difference between the wall and air [43].
R_{window}	The window resistance R_{window} is determined with the window area and the assumption of a heat transmission coefficient $u = 1W/(m^2K)$ [44].
R_{floor}	Heat conductivity and heat convection are the regarded mechanisms to determine the floor resistance R_{floor}. The floor material is reinforced concrete with the thermal conductivity of $2.3W/(mK)$ [45].
R_{inside}	For the convection inside the building, the same assumptions are made as for R_{inside}.
R_{interior}	The interior resistance R_{interior} is also calculated with the heat transfer coefficient inside.

Table 3.3. Explanation of the special material and state dependant values of the differential equation of the inside temperature

Envelope Temperature:

The envelope temperature is influenced by the sun, the contact of the walls with the inner air temperature and with the outside temperature. The sun affects the air temperature differently than the outer walls. Therefore, we differentiate between the influence of the sun on the inner air temperature and the envelope, and we consider here $\dot{Q}_{\text{sun,envelope}}$ in the opposite to Equation 3.3 considering $\dot{Q}_{\text{sun,inside}}$.

$$C_{\text{envelope}} \cdot \frac{dT_{\text{envelope}}}{dt} = \dot{Q}_{\text{sun,envelope}} - \frac{T_{\text{envelope}} - T_{\text{outside}}}{R_{\text{envelope}}} + \frac{T_{\text{inside}} - T_{\text{envelope}}}{R_{\text{inside}}} \tag{3.4}$$

R_{envelope}	The outer wall resistance R_{envelope} contains a heat conductivity of aerated concrete $(0,133 W/(mK)$ [46]) and the heat transfer coefficient for air perpendicular to the wall outside α_{envelope} according to the rules of thumb from Schweizer-fn $\alpha_{\text{envelope}} = 3.96(v/L)^{0.5} = 1.669 W/(m^2K)$ [43] with the average wind velocity of Karlsruhe v [47] and the length of the building wall.
C_{envelope}	To determine the capacitance C_{envelope}, we need the volume of the outer walls from the construction plan [37], the density of aerated concrete $(485 kg/m^3)$ and the capacity $(1000\ J/(kgK))$ [46].

Table 3.4. Explanation of the special material and state dependant values of the differential equation of the envelope temperature

Interior and floor temperature:

The differential equations for the interior and the floor temperature only interact with the inside temperature. Hazyuk et al. [28] models also the ground floor as one state. The explanation is that the ground floor has no convective contact with the environment. Therefore, the ground floor is not modelled with the envelope for receiving the correct physical description, where the wind has an impact on the outer walls. The interior is modelled to improve the accuracy of the inside temperature equations because of the special consideration of the capacitance of the inner walls.

$$C_{\text{interior}} \cdot \frac{dT_{\text{interior}}}{dt} = \frac{T_{\text{inside}} - T_{\text{interior}}}{R_{\text{interior}}} \tag{3.5}$$

$$C_{\text{floor}} \cdot \frac{dT_{\text{floor}}}{dt} = \frac{T_{\text{inside}} - T_{\text{floor}}}{R_{\text{floor}}} \tag{3.6}$$

As above, we have to determine the material parameters of the capacitance C_{floor} and C_{interior}. The material of the floor is reinforced concrete and the interior' material is aerated concrete. The previously unnamed material parameters are the density $(2500 kg/m^3)$ [45] and the capacity $(880 J/(kgK))$ [48] of reinforced concrete.

Summarising, Figure 3.2 illustrates the building model with all connections according to the RC- analogy.

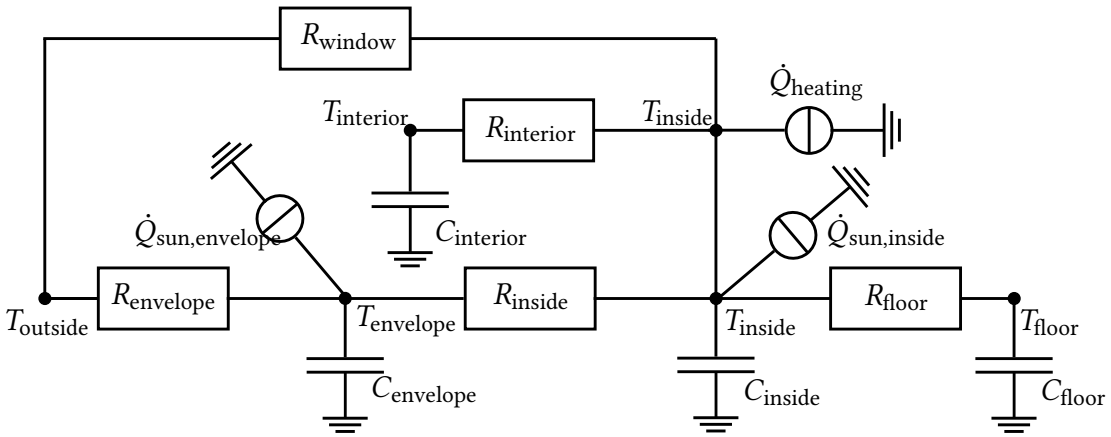

Figure 3.2. Structure of the thermal model in RC- analogy

3.3.1. Parameter identification

Figure 3.3 explains the procedure, how to generate the grey-box model from the physical building model.

We use the MATLAB toolbox "System Identification Toolbox". For this application, the most

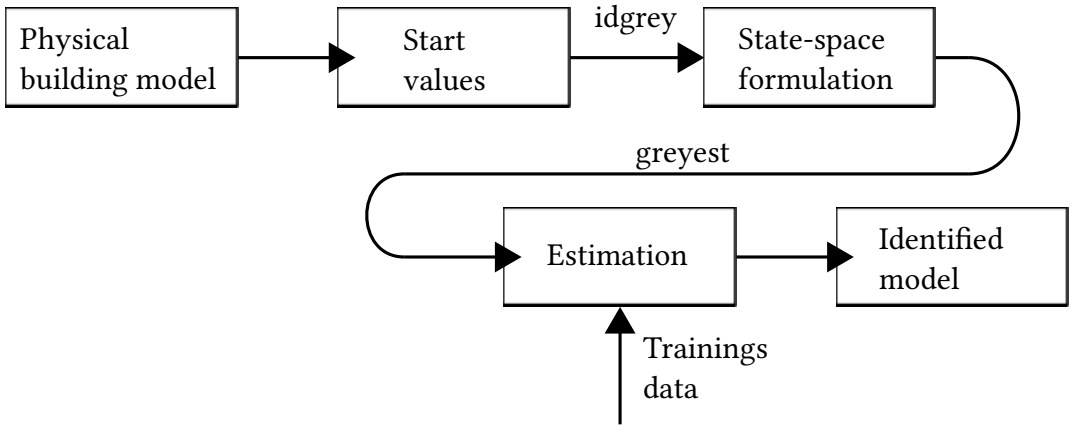

Figure 3.3. Workflow of grey-box modelling with Matlab

important functions are "idgrey" and "greyest". With the idgrey-function, we can specify the building model as the initial model for the grey-box estimation in state-space formulation. That means the thermal resistances and capacitance, which we determined above, are the start values for the estimation and they are the values, which the estimator from Matlab changes. We also identify the parameters $f_{sol,inside}$ and $f_{sol,envelope}$ because we model in the

simplest way the heat flow of the sun insolation $\dot{Q}_{\text{sun,envelope}}$ and $\dot{Q}_{\text{sun,inside}}$ with the measured diffuse insolation I_{sun} (see the following equation).

$$\begin{aligned} \dot{Q}_{\text{sun,inside}} &= f_{\text{sol,inside}} I_{\text{sun}} \\ \dot{Q}_{\text{sun,envelope}} &= f_{\text{sol,envelope}} I_{\text{sun}} \end{aligned} \tag{3.7}$$

The start values for $f_{\text{sol,inside}}$ and $f_{\text{sol,envelope}}$ are chosen as 0.25 according to Harb et al. [12]. We replace in the differential equation of the envelope temperature from Equation 3.4 the thermal resistance R_{inside} to R_{in}. The start values of R_{inside} and R_{in} are the same, but we obtain more flexibility in the grey-box model, if we estimate both values.
Then, we require the data from the reference building. The data is generated in an experiment, as explained in a subsequent chapter. When we have the data, it is separated into training data and verification data. The training data is used for the estimation. From the reference building, we obtain the room temperatures, which we average with the capacitance of each room to one value, the inside temperature. The same procedure is adopted for the outer wall temperature, except that the outer wall temperatures are averaged with their own capacitance. The interior and the floor temperatures are determined in the same way. Also, we obtain data of the heating system for $\dot{Q}_{\text{heating}}$ and the weather (the outside temperature T_{outside} and the diffuse insolation I_{sun}).
Now, the greyest-function executes the parameter identification with the training data. The used search method of the greyest-function is subspace Gauss-Newton least squares search. The table below summarises the modelling parameters for the estimation. The states T_{inside} and T_{envelope} are also defined as the output to be optimised. For the later MPC, T_{inside} is the only relevant output. However, when optimising the two states with the more complex differential equations, we expect better results for the overall model due to the better physical description. At last, we obtain the ready model (see in section A.1 the start values and the identified values).

3.3.2. Training and verification of the thermal model

The training data set contains twelve days from 23 July to 4 August 2021, including a heating period from 26 July to 1 August 2021. The verification data set is half the size of the training data set (from 13 July to 19 July 2021), also including a heating period from 16 July to 18 July 2021.

Parameters to be identified	C_{inside}, C_{envelope}, C_{interior}, C_{floor}, R_{inside}, R_{window}, R_{envelope}, R_{interior}, R_{floor}, R_{in}, $f_{\text{sol,inside}}$, $f_{\text{sol,envelope}}$
Inputs	$\dot{Q}_{\text{heating}}$, I_{sun}, T_{outside}
Outputs to be optimised	T_{inside}, T_{envelope}

Table 3.5. Conclusion of relevant information about the grey-box model

Figure 3.4 and Figure 3.5 show the curve of the inside temperature of the simulated and the

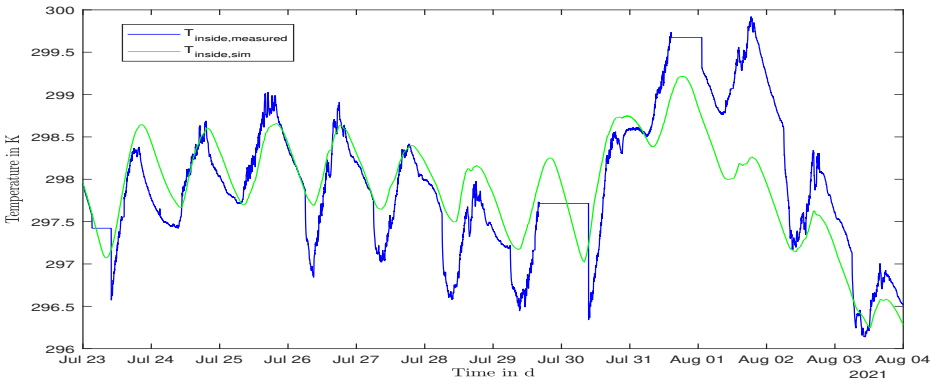

Figure 3.4. Training of the building model

measured values for the training and verification period. The use of data from an occupied building leads to the difference between the model and the measured inside temperature. The required simple model can not consider random influences such as opening doors and windows, the number of occupants, and the electric consumption in the building. Nevertheless, it can be stated that the model sufficiently well reflects the dynamics of reality. In addition, the Root Mean Square Error (RMSE) and the maximum residual (R_{max}) is used as verification measure of the model.

The RMSE is calculated with the quadratic difference of the simulated output y_{sim} and the measured output y_{meas} as follows [49]:

$$RMSE = \sqrt{\frac{1}{N}\sum_{1}^{N}(y_{\text{sim}} - y_{\text{meas}})^2} \tag{3.8}$$

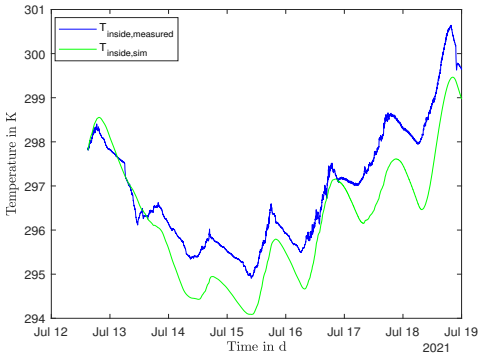

Figure 3.5. Verification of the building model

Here is N the number of measurements or simulated values. Based on RSME and R_{max} in Table 3.6, it can be shown that during the training and verification period, the magnitudes of the RSME and R_{max} are similar. The results of the RMSE and the R_{max} are listed for the two optimised outputs after the training and the verification period. The maximum difference

	T_{inside}		$T_{envelope}$	
RMSE	0.52 K	0.84 K	0.49 K	0.51 K
R_{max}	1.66 K	1.92 K	1.21 K	1.00 K

Training period
Verification period

Figure 3.6. RMSE and R_{max} of the output for training and verification period

between the training and verification period for the RMSE is 0.32 K and in case of the R_{max} 0.26 K. As a result, the building model is verified.

3.4. The state-space formulation

The white-box model of the water reservoir and the grey-box model of the building behaviour have now been prepared. In the next step, we put them together in the state-space formulation, which we introduced in subsection 2.3.2.
To this end, we separate in control signal **u** and disturbances **d**. The control signals are the heat flow of the heating system $\dot{Q}_{heating}$ and the heat pump in the reference building $\dot{Q}_{HP}$.

The main disturbances are the weather and, especially for the water reservoir, heat losses. Therefore, the state-space formulation results as follows:

$$\begin{pmatrix} \frac{dT_{\text{inside}}}{dt} \\ \frac{dT_{\text{envelope}}}{dt} \\ \frac{dT_{\text{interior}}}{dt} \\ \frac{dT_{\text{floor}}}{dt} \\ \frac{dU_{\text{WR}}}{dt} \end{pmatrix} = A \begin{pmatrix} T_{\text{inside}} \\ T_{\text{envelope}} \\ T_{\text{interior}} \\ T_{\text{floor}} \\ U_{\text{WR}} \end{pmatrix} + B_1 \begin{pmatrix} \dot{Q}_{\text{heating}} \\ \dot{Q}_{\text{HP}} \end{pmatrix} + B_2 \begin{pmatrix} I_{\text{sun,inside}} \\ I_{\text{sun,envelope}} \\ T_{\text{outside}} \\ \dot{Q}_{\text{loss}} \end{pmatrix} \tag{3.9}$$

$$T_{\text{inside}} = C \begin{pmatrix} T_{\text{inside}} \\ T_{\text{envelope}} \\ T_{\text{interior}} \\ T_{\text{floor}} \\ U_{\text{WR}} \end{pmatrix}$$

The complete matrices A, B_1, B_2, and C are presented in section A.2. We have no pass-through matrices D_1 or D_2 because neither control signals nor disturbances have a direct impact on the output.

4. Experiments

In section 3.3, it is described how the grey-box model of the building is created. However, it is not precisely explained where the data comes from. Experiments have been conducted specifically to obtain this data. These experiments are explained in this chapter.
This thesis is developed during the summer, thus no data from the reference building with a non-zero control signal $\dot{Q}_{\text{heating}}$ are available. To acquire data with the varying control signal, we heat the reference building with electric heaters in two experiments, one for the verification data and one for the training data. Therefore, the sensors of the building record the temperature curves in the rooms and the electrical consumption of the building. The experiments are under the assumption that the whole electrical power of the heaters and other consumers of power, such as lights and office devices, is converted to heat.

4.1. Experiment 1

The feasibility of the first experiment on the reference building is unclear. To be able to simply repeat the experiment in the event of an error, the experiment with the smaller data set is conducted at first. Hence, the first experiment aims to obtain the data for the verification period, which is shorter than the training period. Furthermore, the experiment is conducted over a weekend (from 16. July to 18. July 2021), as we reduce interference from occupants, such as opening doors or windows, and we enable the occupants a comfortable working temperature. Therefore, all windows and doors are opened after the experiment to cool down the building. At last, there should be no electrical charging of the cars during the experiment, because this electricity consumption has the same measuring point as the electricity consumption of the entire building. This would disrupt the assumption that all electrical power is converted into heat.
At first, we set up the household heater without a fan in room 1, the household heater with a fan in room 2, and the industrial heater in floor 2 (see Figure 2.4). The heaters are

Heater	Acronym	Technical data	Configuration
Household Heater without a Fan	HoHe	• maximum power: 2000W • closed-loop control	• switch symbol: | • temperature setting: $5-6$
Household Heater with a Fan	HoHeF	• maximum power: 2000W • open-loop control	• switch symbol: 750W
Industrial Heater	IH	• maximum power: 9000W • closed-loop control • three phase	• switch symbol: ▬ • temperature setting: middle

Table 4.1. Technical data and configuration during the experiments [50], [51], [52]

selected based on availability so that no new equipment has to be purchased. Some technical information and the configuration of the heaters are described in Table 4.1.

4.1.1. Data of the experiment 1

A more exact sequence of the experiment is shown in Table A.2 as laboratory journal or in Figure 4.1 with the data. The Figure presents the electrical consumption P_{el} and the air temperatures in rooms 1 and 2, the kitchen, and floor 2 of the reference building from the beginning to the ending of the experiment. The start is marked by switching on the heaters in floor 2 and rooms 1 and 2. In the end, the heaters are switched off in room 1, the kitchen and floor 2.
The data demonstrate the behaviour of the heaters. Consequently, in floor 2, the IH switches often on and off due to the closed-loop control. Therefore, IH generates the fluctuations in the increasing air temperature curve. At the same time, we notice the on and off of the heater in P_el at the high peaks. The HoHe has the same behaviour as the IH but with a smaller influence on the air temperature in room 1 due to its lower power.
Only the HoHeF is controlled open-loop and heats constantly with 750W the room air, where

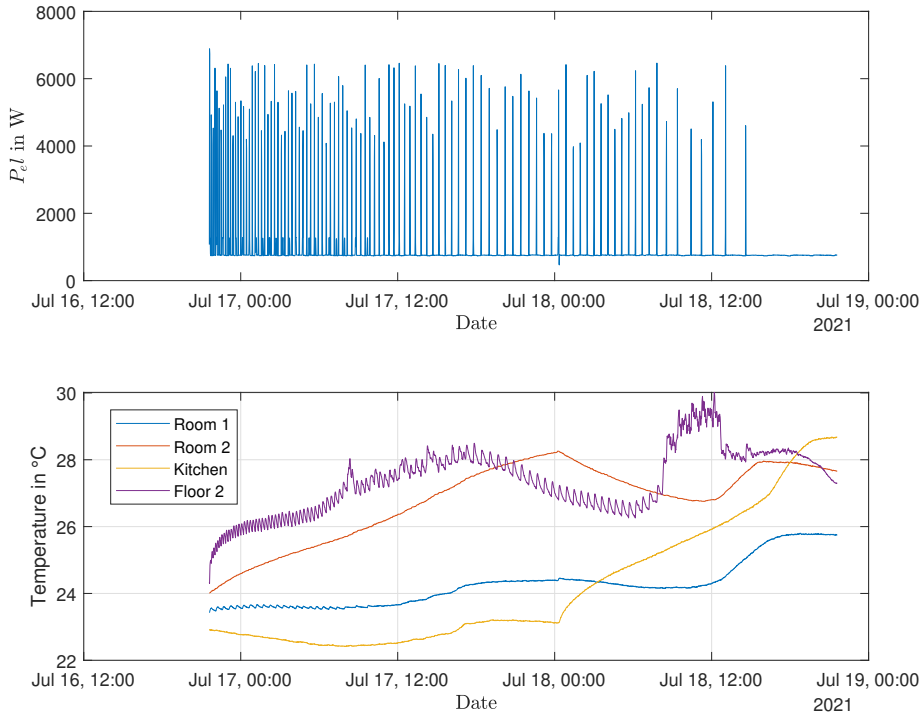

Figure 4.1. Electrical consumption of the building and air temperature inside the rooms during the experiment 1

we remark no fluctuations in the temperature rise. Because the HoHeF does not switch off independently and we have sunny days during the experiment, some temperatures, e.g. the screed temperature, are close below 40°C. To avoid a too-hot room for the occupants after the experiment, we stop heating room 2 on Saturday night and rearrange the HoHeF in the kitchen. Since we average the temperature in all rooms for the model estimation from chapter 3, it is not relevant which room is heated.

4.2. Experiment 2

Experiment 2 roots also on the general assumption of converting the entire electrical power to heat, and starts on Monday, 26. July 2021 and ends on Sunday night, 1. August 2021. We use also the heaters explained in Table 4.1. In contrast to experiment 1, we can now remotely control the switching on and off of the heaters due to an update in the building. Therefore, we can generate more training data by controlling heating periods on working days during the

night and on the weekend. In order not to burden the occupants during the working day, we heat at night and only the unused kitchen with the HoHeF. In addition, we can use another measuring point for the electrical consumption during the working days, where the electric car charging is not considered. Only for the weekend, we need both measuring points (the one only used in experiment 1 and the new one used during the working days in experiment 2) to measure the whole energy consumption because of the three-phase connection of the IH, which is measured at the same point as car charging. So, we have to ensure no car charging during the weekend. Besides, the heaters are in the same rooms as in experiment 1 over the weekend. Table A.3 or the data describe the incidences during experiment 2, which is explained in detail in the next section.

4.2.1. Data of the experiment 2

Figure 4.2 presents the needed electrical consumption and the air temperatures of the rooms of interest during experiment 2. Especially, the air temperature of the kitchen is showed over the whole experimental phase because in the first five days only this room is heated for reasons explained above. The heating periods are remarked by horizontal lines. The visible horizontal curves of the air temperatures arise from the breakdown of the programmable logic controller (PLC) . During this breakdown, no temperature data can be recorded. In every heating period with a working PLC, the increasing temperatures are conspicuous. Notice the third period: The rising temperature is visible from the point at closing the door in the kitchen (compare Table A.3). When the door is open, the heat spreads in the building and, a smaller temperature rise is visible in the kitchen. In this experiment, also, the different heaters have the same effect on the air temperatures and the HoHeF is moved from room 2 to the kitchen to avoid too high temperatures at the weekend.

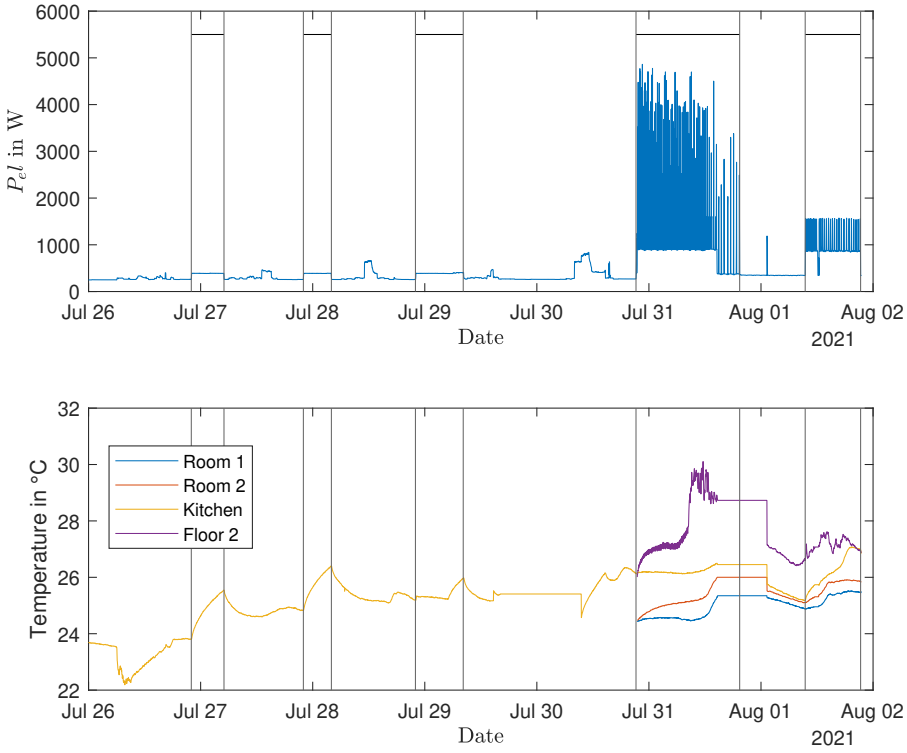

Figure 4.2. Electrical consumption of the building and air temperature inside the rooms during the experiment 2

4.3. Findings of the experiments

All influences on the building are noticeable in the data. The heating of a room directly increases the air temperature and with a time delay the wall and screed temperatures; the room temperature rises more slowly through open inner doors; the temperature curves show whether the heater is heating or not; and opening all windows and doors lead to a decreasing temperature at the end of the experiments.

No temperature data can be recorded during the PLC breakdown. This degrades the quality of the data used to estimate the model. Especially during this time, it is partially heated. Data collection would be particularly important here to determine the influence of heating. To reduce the negative impact on the data, it is important to switch off the heaters quickly in case of PLC breakdown, which is possible with remote access for the household heaters. This

does not apply to the IH, as it has no remote control due to its three-phase connection and thus heats for longer periods without temperature detection.
In a look back, the use of different measuring points for electrical consumption is disadvantageous. If it seemed advantageous when considering experiment 2 that no consideration has to be given to the car charging, this actually means that the same combination of measuring points has to be used for the verification data from experiment 1, which was not planned, at first. Therefore, the model is identified with the sum of the data from both measuring points, within a period of car charging. Nevertheless, we obtain a suitable model for the MPC.

5. Model predictive control

In this chapter, the framework conditions of the MPC are described by answering the questions: (i) what is controlled? (ii) How is it controlled? (iii) Which curves are controlled? (iii) What data is used? Additionally, the constraints, the cost function, and the workflow of the MPC script are introduced. The objective of this investigation is to obtain a control signal for the heat pump of the reference building that considers grid services and occupancy comfort. There, the investigation stays in a simulation environment.

5.1. Framework conditions of the MPC

The objective of the MPC is to optimise the control signal of the reference building $\mathbf{u} = (u_1 \;\; u_2)^T = (\dot{Q}_{\text{heating}} \;\; \dot{Q}_{\text{HP}})^T$. Thereby, we consider the heat flows of the building in the MPC simulation. To investigate DSM, we require an impact on the grid of the control signal. Therefore, we subsequently calculate the electrical control signal P_{HP} using the characteristic diagram of the heat pump from the $\dot{Q}_{\text{HP}}$. The controlled output is the inside temperature $\mathbf{y} = T_{\text{inside}}$, which we calculate with the thermal model from section 3.4. The desired curves of $\mathbf{y}$ depend on the presence of occupants, which is determined by an occupancy schedule. To obtain a simulation environment, we use past data of the weather as the disturbances d_{k} and the dynamic price of the electricity Pr as an indicator for the grid balance. The characteristic diagram, the occupancy schedule, and the used data are introduced in the following subsections.

5.1.1. Characteristic diagram of the heat pump

The characteristic diagram of the heat pump is interpolated from the characteristic values specified by the producer [40]. We assume an operation at the nominal power of the heat pump. As Figure 5.1 shows, the electrical power P_{HP} depends on the outside temperature

T_{outside} and the required heat flow $\dot{Q}_{\text{HP}}$. Further, the heat pump can generate negative heat flows when cooling is desired. The optimisation of the MPC computes $\dot{Q}_{\text{HP}}$, and T_{outside} is known at every time step, hence the characteristics of the heat pump are used to calculate P_{HP}. Since the control signal is a heat flow, the effects on the grid cannot be assessed directly. Therefore, P_{HP} is needed to analyse the effects on the grid. Furthermore, converting $\mathbf{u}$ into P_{HP} simplifies the analysis, as we then only consider positive values.

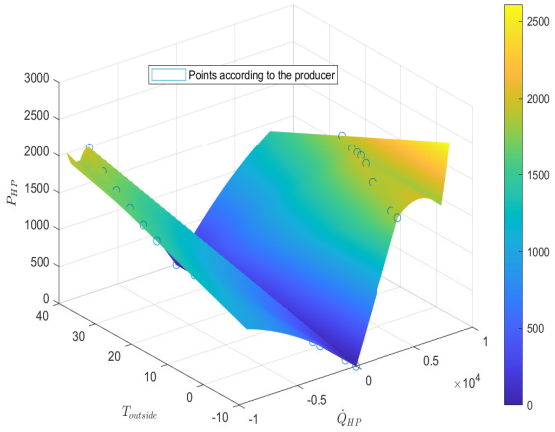

Figure 5.1. ~~Interpolation of the~~ characteristic diagram of the heat pump with nominal power accor[illegible]g to [40]

5.1.2. Occupancy schedule

Since the reference building is used as an office, the occupancy schedule describes at which day and time persons work in the reference building. We use the schedule as a specification when the comfort should be considered in the MPC. Figure 5.2 shows the occupancy schedule. It summarises the working time of occupants with a green bar. We assume that persons are in the reference building from Monday to Thursday from 6 am to 7 pm and on Friday from 6 to 6 pm. The assumption is based on experience values and means that there is a high probability that persons will be in the building during this time.

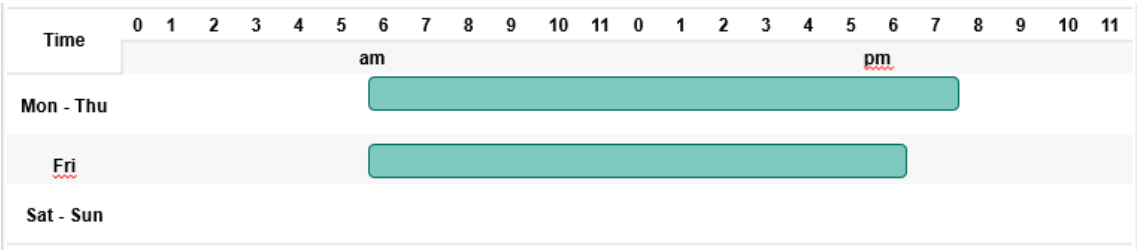

Figure 5.2. Occupancy schedule of the reference building

5.1.3. Used data

In a real applied MPC, we would use weather forecast as the disturbances d_k in the state-space formulation for calculating the future behaviour of the system with the optimal control signal. Since we only simulate the behaviour of the building, we can use past data of the weather as d_k.

The data used is from the same period as the training data for the model estimation. As the disturbance variable, we use the recording of diffuse radiation and outside temperature in Energy Lab 2.0. The MPC is simulated over nine days, to consider the full occupancy schedule at least once.

The dynamic price of the electricity Pr is made available on the website of the Bundesnetzagentur [53]. Here we use the wholesale prices on the stock exchange as an indicator of grid services. The price is an intersection ~~between~~ supply and demand. Consequently, when the price is low, we can assume an excess of electricity in the grid. Then it is particularly suitable to operate our heat pump to obtain electricity from the grid. In the opposite case, the same applies: If the price is high, it is unfavourable to operate the heat pump. At such times, it is particularly suitable to supply power from the grid.

However, negative prices can also arise in retail. Negative prices would undesirably change the cost function, which will be explained in detail later with reference to the cost function. To avoid negative prices, we add the absolute minimum value of Pr to every value of Pr. Thus, we shift the curve of Pr into positive, as shown in Figure 5.3. Henceforth, we will utilise the dynamic price of electricity Pr in the unit of $\frac{€}{Wh}$.

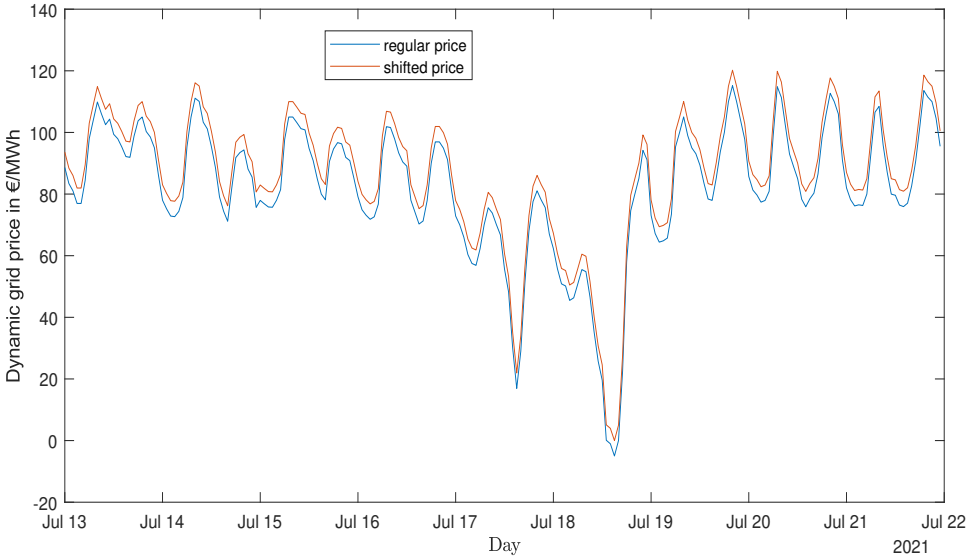

Figure 5.3. Dynamic price of electricity [53] and shifted dynamic price of electricity

5.2. The Constraints

We generally define in subsection 2.3.3 constraints. Further, we differ soft and hard constraints in the following. The hard constraints depend on the physical limitations of the installations in the building, such as the heat pump, the underground floor heating, and the water reservoir. The used soft constraint in this MPC smooths deviations ~~of a comfortable~~ temperature range. Further, the integration method of the model is included in the constraints to calculate the future states over one horizon. The subsequent section gives an overview of the constraints regarding the control signal, the output, the states, and an introduction of the integration method.

5.2.1. Constraints of the control signals

The control signals are ~~hard~~ constrained by the physical limitations of the heat pump, the underfloor heating and the cooling configurations.
The producer's specifications restrict $\dot{Q}_{\mathrm{HP}}$ for nominal power by an inlet temperature of 55°C in case of heating and by an inlet temperature of 18°C in case of cooling [40]. The maximum $\dot{Q}_{\mathrm{heating}}$ is limited according to the underground floor heating calculation, where the set power of every room is counted and summed for the complete building [54]. The computation of the

required cooling power predicts 2246 W needed power in case of 34.5°C outside temperature in July [55]. To be more flexible with higher outside temperatures, we round the minimum $\dot{Q}_{\text{heating}}$ to 2300 W.
Further, we define a constraint $u_1 \cdot u_2 \geq 0$ to avoid simultaneous heating of building and cooling of the water reservoir or reversed as this would waste energy needlessly. The set $\mathbb{U}_{\mathbb{k}}$ summarise mathematically the constraints.

$$\mathbb{U}_{\mathbb{k}} = \{\mathbf{u_k} | -2300W \prec \dot{Q}_{\text{heating}} \prec 5283W \wedge -9340W \prec \dot{Q}_{\text{HP}} \prec 8010W | u_1 \cdot u_2 \geq 0\} \tag{5.1}$$

5.2.2. Constraint of the output

We specify a comfortable temperature range with the soft constraint of the output. The following explains the range of a comfortable temperature.
The Umweltbundesamt [56] recommends an inside temperature of 18°C for some rooms, such as the kitchen. We expand the recommendation to a minimum T_{inside} of 18°C for all rooms. The maximum inside temperature refers to the German technical rules for workplaces [57], wherein a maximum of 26°C as room temperature is prescribed. The slack variable η_{k} allows a variance of the given temperature range during a penalty in the cost function. Thus, we have a soft constraint, and we can obtain the feasibility of the optimisation problem during a deviation of the temperature range [58]. The constraint is represented in the set $\mathbb{Y}_{\mathbb{k}}$ as follows:

$$\mathbb{Y}_{\mathbb{k}} = \{\mathbf{y_k} | 18°\text{C} - \eta_k \prec T_{\text{inside}} \prec 26°\text{C} + \eta_k\} \tag{5.2}$$

5.2.3. Constraints of the states

We only have to constrain the state of the water reservoir because of its physical limitation. Therefore, we use a hard constraint. The calculation of the water reservoirs maximal inner energy U_{WR} is explained in section 3.2 with Equation 3.2. The minimum U_{WR} is 0 J. The set $\mathbb{X}_{5,k}$ describes the constraint for the fifth element of the state vector.

$$\mathbb{X}_{5,k} = \{x_{5,\text{k}} | 0J \prec U_{\text{WR}} \prec 96370000J\} \tag{5.3}$$

A further constraint, which relates to the states, is the integration method as discussed below.

5.2.4. Integration method and its constraint

As an integration method, we use a explicit single-step method, which means that we only need the values of the current time step k to compute the next. Possible methods are the Heun's method, the Euler and the Runge-Kutta method. The decision is made in favor of the fourth-order Runge-Kutta method because the fourth order makes it more precise at a given step size than the other methods mentioned above. The following equation shows the integration scheme using the Runge-Kutta method with the sample time T_s and the function $f(\mathbf{x_k}, t_k, \mathbf{u_k}, \mathbf{d_k}) = \mathbf{x}_k$ according the state-space formulation (see Equation 2.20) [59].

$$
\begin{aligned}
a_k^{(1)} &= T_s \cdot f(\mathbf{x_k}, t_k, \mathbf{u_k}, \mathbf{d_k}) \\
a_k^{(2)} &= T_s \cdot f(\mathbf{x_k} + \frac{a_k^{(1)}}{2}, t_k + \frac{T_s}{2}, \mathbf{u_k}, \mathbf{d_k}) \\
a_k^{(3)} &= T_s \cdot f(\mathbf{x_k} + \frac{a_k^{(2)}}{2}, t_k + \frac{T_s}{2}, \mathbf{u_k}, \mathbf{d_k}) \\
a_k^{(4)} &= T_s \cdot f(\mathbf{x_k} + a_k^{(3)}, t_k + T_s, \mathbf{u_k}, \mathbf{d_k})
\end{aligned}
\tag{5.4}
$$

$$
\mathbf{x_{k+1}} = \mathbf{x_k} + \frac{1}{6} \cdot (a_k^{(1)} + 2a_k^{(2)} + 2a_k^{(3)} + a_k^{(4)})
$$

The constraints accommodate the integration method for calculating the next time step according to the determined thermal model. Important to note is that the time step of the integration is chosen in accordance with the discretization of the model. The model is estimated with the discrete values of the reference building, where the measuring points are sampled every two minutes. For example, to achieve a T_s of one hour, T_s is described as $30 \cdot 2min$. The two minutes are already included in the model by estimation. Therefore, we multiply $\mathbf{x}_k$ by 30 to bring forward a time step of one hour. It is considered that the thermal model is composed of two submodels. The water reservoir sub-model, which is modelled using the white-box approach, requires a different conversion to advance one hour. Here we convert watts to joules per hour. In the MPC, this difference is compensated by a factor directly in the state-space formulation of the model.

5.3. The Cost function

The cost function penalises the deviation from the desired requirements. On the one hand, we have to guaranty thermal occupant comfort in the building. On the other hand, we prefer to heat with the heat pump during convenient grid service. Both subjects are represented in the cost function below with the weightings w_1 and w_1, which relate to the requirements comfort and grid services.

$$\text{minimize} \sum_{k=1}^{N-1} w_1 \cdot (y_\text{k} - y_\text{track})^2 + w_2 \cdot (u_{2,\text{k}} \cdot Pr_\text{k})^2 + w_3 \cdot \eta_\text{k}^2 \tag{5.5}$$

At first, we determine the desired temperature y_track of the comfort requirement in the cost function. A pleasant air temperature is 22°C for living rooms, working rooms, and the bathroom [56]. As discussed in chapter 3, we model the reference building as a single-zone building, wherein most rooms are working rooms. We decide to use the median temperature of all rooms of the recommended temperatures for the complete building. Thus, the desired temperature is $y_\text{track} = 22°\text{C}$.
The expression $(y_\text{k} - y_\text{track})^2$ represents the comfort requirement in the cost function. The squaring of $(y_\text{k} - y_\text{track})$ avoid a minimising of the cost function due to negative $(y_\text{k} - y_\text{track})$ values. The same is applied to the expression of the grid service $(u_{2,\text{k}} \cdot Pr_\text{k})^2$. We exclude negative values of Pr_k (as explained in subsection 5.1.3) because they would generate an incorrect effect. Then after squaring, the expression $(u_{2,\text{k}} \cdot Pr_\text{k})^2$ would maximise the cost function during a appropriate time for grid services due to a negative Pr_k. Without a squaring, we would support energy consumption while its not needed or we would penalise a cooling by we having a negative $u_{2,\text{k}}$ multiplied with a negative Pr_k.
We can adjust the preference of the requirements comfort and grid services by the weightings w_1 and w_2. How much deviation is allowed from the temperature range in the soft constraint is determined by the weighting w_3.
The magnitude of the costs of the requirements are different. When considering the constraints, $y_\text{k} - y_\text{track}$ can reach a maximum deviation of 4 K (without soft constraint), while $u_{2,\text{k}} \cdot Pr_\text{k}$ is in a lower order of magnitude due to the unit $\frac{€}{Wh}$. To compensate for this, a factor is introduced that gives the comfort requirement a weaker weighting in the cost function. The factor is integrated into the weighing w_1 as shown in the following table. In general, we vary the weights w_1 and w_2 of the cost function from $i_1 = 0$ to 1 in steps of 0.1. As shown in table

Table 5.1, the comfort with w_1 and the grid service with w_2 are always weighted in opposite directions.

Occupant comfort is only necessary if persons are present in the building. Therefore, we

w_1	w_2	w_3
$\frac{1}{4} \cdot i_1$	$i_2 = 1 - i_1$	0.01

Table 5.1. Weighting factor

consider the cost function during absence without the comfort requirement by setting w_1 to zero according to the occupancy schedule, which results in the following simplification of the cost function during absence.

$$\text{minimize} \sum_{k=1}^{N-1} w_2 \cdot (u_{2,\mathrm{k}} \cdot Pr_{\mathrm{k}})^2 + w_3 \cdot \eta_{\mathrm{k}}^2 \tag{5.6}$$

The procedure aims to generate more flexibility for the objective of grid services. We define this scenario with the changing cost function as the basic scenario for this thesis, which is needed in the following chapter.

5.4. Workflow of the MPC script

The approach in the MPC script is determined by the use of the tool CasAdi. CasADi is an open-source tool for nonlinear optimisation and algorithmic differentiation and is characterised by a symbolic framework. Mixed-integer optimal control problems, such as an MPC, are of particular interest [60]. We can combine CasAdi with MATLAB through a simple import.
Figure 5.4 gives an overview of the workflow of the MPC script. First, we declare the parameter, all known sizes, and the optimisation variables symbolically. Then the inequalities of the constraints are set in a loop over the prediction horizon with the symbolic variables. The cost function is also indicated symbolically for the horizon. Afterwards, the initial values for the optimiser are determined. To specify the initial state for the first MPC step, we choose a constant control signal $\mathbf{u_k} = [0 \;\; 0]^T$, a state $\mathbf{x}$ within the temperature range, and determine with the Runge-Kutta method the curve over the horizon. A half charged water reservoir constitutes a further assumption for the initial state. We pass the values of the initial state of the optimisation variations and the parameters to the solver. Then, the optimisation problem is solved with the Ipopt (**I**nterior **P**oint **Opt**imiser) solver [60]. As a result, we obtain the

optimised $\mathbf{u_k}$ over the horizon. Now, after each time step, a new initial state is calculated with the curves of the states and the output from the new disturbance variables and the optimum $\mathbf{u_k}$ over the horizon.

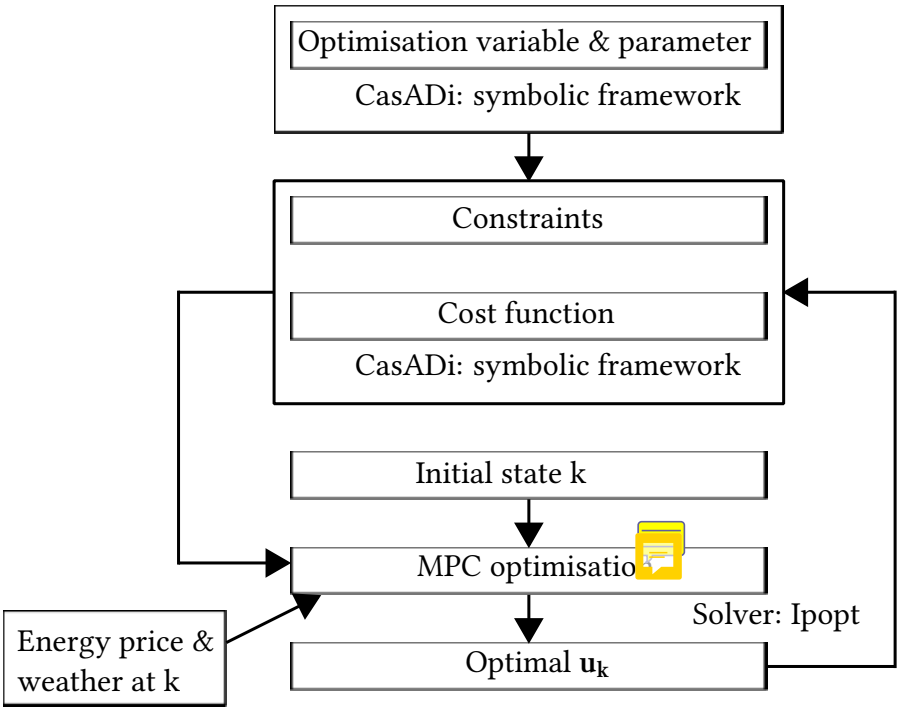

Figure 5.4. Workflow of the MPC script

5.5. Choice of weightings and horizon

In the following, we analyse the horizon length N and the effects of the weightings on the requirement of occupancy comfort and grid services for the basic scenario. For a better comparison we define an average comfort $\Delta\overline{y}$, which is the average deviation of y from y_{track} over the simulation time only during presence of occupants, expressed by $y_{\text{k,occ}} - y_{\text{track}}$. The calculation of $\Delta\overline{y}$ is described in the following equation with the number of time steps with occupants n_{occ}.

$$\Delta\overline{y} = \frac{\sum_{k,occ}^{n_{\text{occ}}} |y_{\text{k,occ}} - y_{\text{track}}|}{n_{\text{occ}}} \tag{5.7}$$

On the other hand, we define the costs for grid services (GS) over the whole simulation time (with the number of time steps n) as the sum of the electrical power of the heat pump $P_{\mathrm{HP,k}}$ multiplied with the dynamic price of electricity Pr_{k}:

$$GS = \sum_{k}^{n} P_{HP,k} \cdot Pr_{\mathrm{k}} \tag{5.8}$$

In theoretical considerations, we should obtain a higher value of $\Delta\overline{y}$ with less weighting of comfort and a higher value of GS with less weighting of grid services. Furthermore, a larger or shorter horizon N differs in computation time and finding the optimal solution. While a longer N requires more computation time and may not find a solution, a shorter N may not find the optimal solution. Due to finding the optimal solution a larger horizon should result in less costs for the requirements. In general, the horizon should depict the dynamics of the controlled system.
The theoretical considerations are inspected in the subsequent sections for the basic scenario over the simulation time of nine days.

5.5.1. Average comfort and grid services over the weightings

The following figure presents the behaviour of $\Delta\overline{y}$ and GS for the different weightings w_1 and w_2 with $N = 24h$. We also compare the behaviour for different horizon N to verify the feasibility and the expected behaviour. The corresponding figures are shown in section A.4 and the values of $\Delta\overline{y}$ and GS for different horizons are displayed in the following tables.
We notice a monotone behaviour of the average comfort and the grid services according to their weightings apart from small discrepancies. A possibility for discrepancies could be that the optimiser find not the global optimum. We obtain feasible solutions apart from $N = 12h$ and both weightings are 0.5. The lower costs with increasing horizon length are only for the average comfort notable, expecting the case $w_1 = 0$. In this case, we consider not the comfort in the cost function. Therefore, the values of $\Delta\overline{y}$ are random, also relating to the horizon length.
The explanation for higher cost in GS with longer horizon is that the thermal reaction of the building is known over a longer time and the control signal reacts early for a better adaption of the comfort.

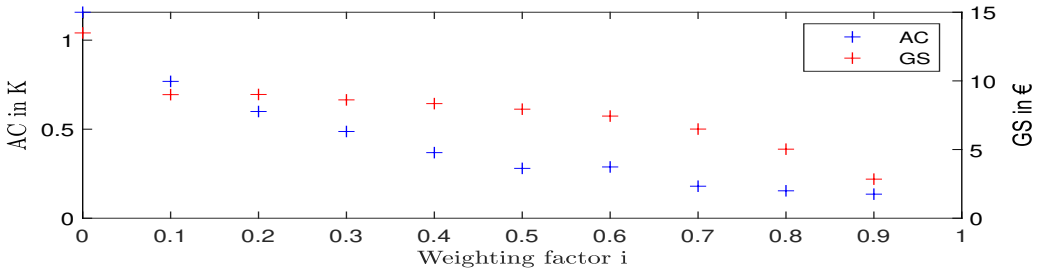

Figure 5.5. $\Delta\overline{y}$ and GS for N = 24h

weighting factor i	0	0.1	0.2	0.3	0.4	0.5	0.6	0.7	0.8	0.9	1
$\Delta\overline{y}$ by N = 12 h	1.11	0.89	0.77	0.64	0.54		0.40	0.28	0.24	0.22	0.22
$\Delta\overline{y}$ by N = 18 h	1.14	0.80	0.72	0.54	0.43	0.35	0.41	0.24	0.17	0.16	0.14
$\Delta\overline{y}$ by N = 24 h	1.16	0.77	0.60	0.49	0.37	0.28	0.29	0.18	0.15	0.14	0.20
$\Delta\overline{y}$ by N = 30 h	1.16	0.75	0.55	0.42	0.31	0.25	0.22	0.18	0.16	0.14	0.16

Table 5.2. $\Delta\overline{y}$ for different N

weighting factor i	0	0.1	0.2	0.3	0.4	0.5	0.6	0.7	0.8	0.9	1
GS by N = 12 h	11.97	8.31	7.90	7.35	6.93		5.23	4.37	3.12	1.71	0.00
GS by N = 18 h	16.45	9.16	8.76	8.57	7.61	7.57	6.77	5.68	4.05	2.39	0.00
GS by N = 24 h	13.50	9.00	9.01	8.62	8.35	7.94	7.44	6.49	5.03	2.85	0.00
GS by N = 30 h	13.74	8.82	8.81	8.56	8.65	8.13	7.48	6.62	5.28	3.39	0.00

Table 5.3. GS for different N

5.5.2. Choice of the horizon

A predictive horizon should depict the dynamics of the system, in this case, the temperature profile inside the reference building. Therefore, the following figure shows T_{inside} of the

building over three days determined from the measurements as a single-zone building as explained in chapter 3. We notice around every 24 h a periodic wave in the temperature profile, which is highlighted with vertical lines.

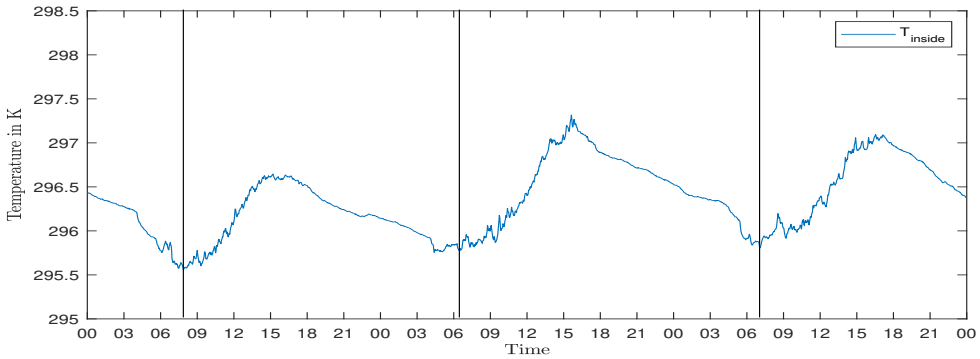

Figure 5.6. Measured data of the reference building: T_{inside} over three days

The wavy profile occurs by day and night fluctuations of the weather. Therefore, Figure 5.6 seems to be an indicator for the dynamics of the system, but the reaction of T_{inside} to a control signal is not illustrated. Nevertheless, we propose a predictive horizon of one day in order to consider complete day and night fluctuations in the predictions. We examine this consideration by comparing costs over different horizons for an exemplary weighting. The following figure shows the curve of costs over the simulation period. The costs here are the sum of comfort and grid services. Here, the comfort according to the occupancy schedule is only considered when the occupants are in the building. Therefore, the peaks are recognizable, and from day four to the beginning of six, there are almost no costs, as this is the weekend. The distinctions in costs at different horizons are as expected. The horizon $N = 12h$ has the highest costs, while with the longer predictions, the costs decrease.
We choose the horizon of 24 h because it represents the dynamic of the reference building and the costs are partly very similar to the next longer horizon of 30 h, e.g. in the last simulation days.

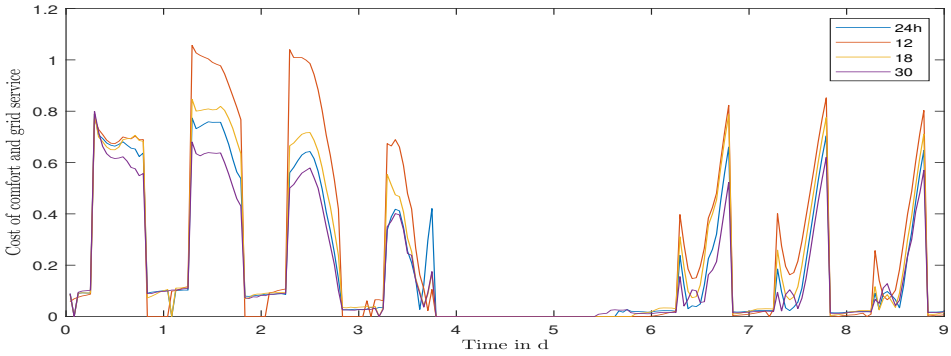

Figure 5.7. Curve of the sum of cost over simulation time for different N

6. Results and discussion

In this chapter, different scenarios are considered to answer the research question focusing on grid services. Several scenarios are supposed to explain how the occupancy schedule affects energy consumption, grid service and comfort: (i) a scenario with an occupancy schedule, in which the MPC has to comply with fewer restrictions during the absence of occupants; (ii) a scenario that also has a lower temperature specification during the absence; and (iii) a scenario without an occupancy schedule. In the last section, the results are evaluated, and an answer to the research question is found.

6.1. Results of the scenarios

In this section, the implementation of the different scenarios is explained and the results of the temperature and control signal curves are presented. Furthermore, energy consumption, comfort and grid services are evaluated.

6.1.1. Presentation of the scenarios

(i) The basic scenario:
The first considered scenario is the basic scenario, which is explained in detail in chapter 5. Summarised, we desire the T_{inside} during the presence of occupants as 22°C. And we leave the optimiser free to find an optimal temperature in the specified temperature range during the absence realised by neglecting the comfort requirement in the cost function.

(ii) Scenario 2:
The Umweltbundesamt [56] recommends during the absence of persons a room temperature of 17°C. Therefore, we consider scenario 2 with the desired T_{inside} during the presence of occupants with 22°C and during absence with 17°C. In the opposite to the basic scenario, we do not change the cost function 5.5 during presence and absence. We switch the y_{track}

between a $y_{\text{track,presence}}$ as 22°C and a $y_{\text{track,absence}}$ as 17°C. We achieve the implementation of scenario 2 using one more symbolic parameter in the optimisation, which is set by the occupancy schedule to $y_{\text{track,presence}}$ or $y_{\text{track,absence}}$. In addition, the temperature range needs to enlarge because the lower bound requires to be under the requested temperature. Thus, we choose 16.5°C as a lower bound. The set of constraints changes to:

$$\mathbb{Y}_{\mathbb{k}} = \{\mathbf{y_k} | 16.5°\text{C} - \eta_k \prec T_{\text{inside}} \prec 26°\text{C} + \eta_k\} \tag{6.1}$$

The MPC algorithm has to handle significant fluctuations of the desired temperature. Therefore, we reduce the weighting w_3 to minimum needed depending on the w_1 and w_2 and adjust the soft constraint. In this way, we allow more deviations of the desired temperature to obtain a feasible solution of the MPC.

(iii) Scenario 3:
Scenario 3 is the simplest optimisation problem. The desired T_{inside} is the 22°C over the complete simulation time. This case does also not consider the occupancy schedule. We can use the cost function 5.5 without changes during the time and all constraints discussed in section 5.2.

6.1.2. Results of the scenarios

To point out the influence of the weightings in the cost function, all results are presented for two representative weights, which enables to focus on the requirements comfort or grid services. The chosen weightings are $i_1 = 0.1 \vee 0.9$ and $i_2 = 0.9 \vee 0.1$. In the following the resulting inside temperature T_{inside}, the control signals $\dot{Q}_{\text{heating}}$ and $\dot{Q}_{\text{HP}}$, and the electrical consumption of the heat pump P_{HP} are shown over the simulation period, as well as the $\Delta\overline{y}$ and GS for every scenario.

Figure 6.1 shows the curves of T_{inside} of the three different scenarios over nine days, the simulation period. The chosen unit for temperatures is Kelvin. According to a conversion of the tracking temperatures in Kelvin, we obtain $y_{\text{track}} = 295.15K$, $y_{\text{track,presence}} = 295.15K$, and $y_{\text{track,absence}} = 290.15K$. We separate between the higher grid service $i_2 = 0.9$ and lower comfort requirement $i_1 = 0.1$ in the above diagram and the lower grid service $i_1 = 0.1$ and higher comfort requirement $i_1 = 0.9$ in the below diagram.

The inside temperature curve of scenario 2 runs below T_{inside} of both other scenarios. Scenario 3 is closer to the y_{track} than the basic scenario.

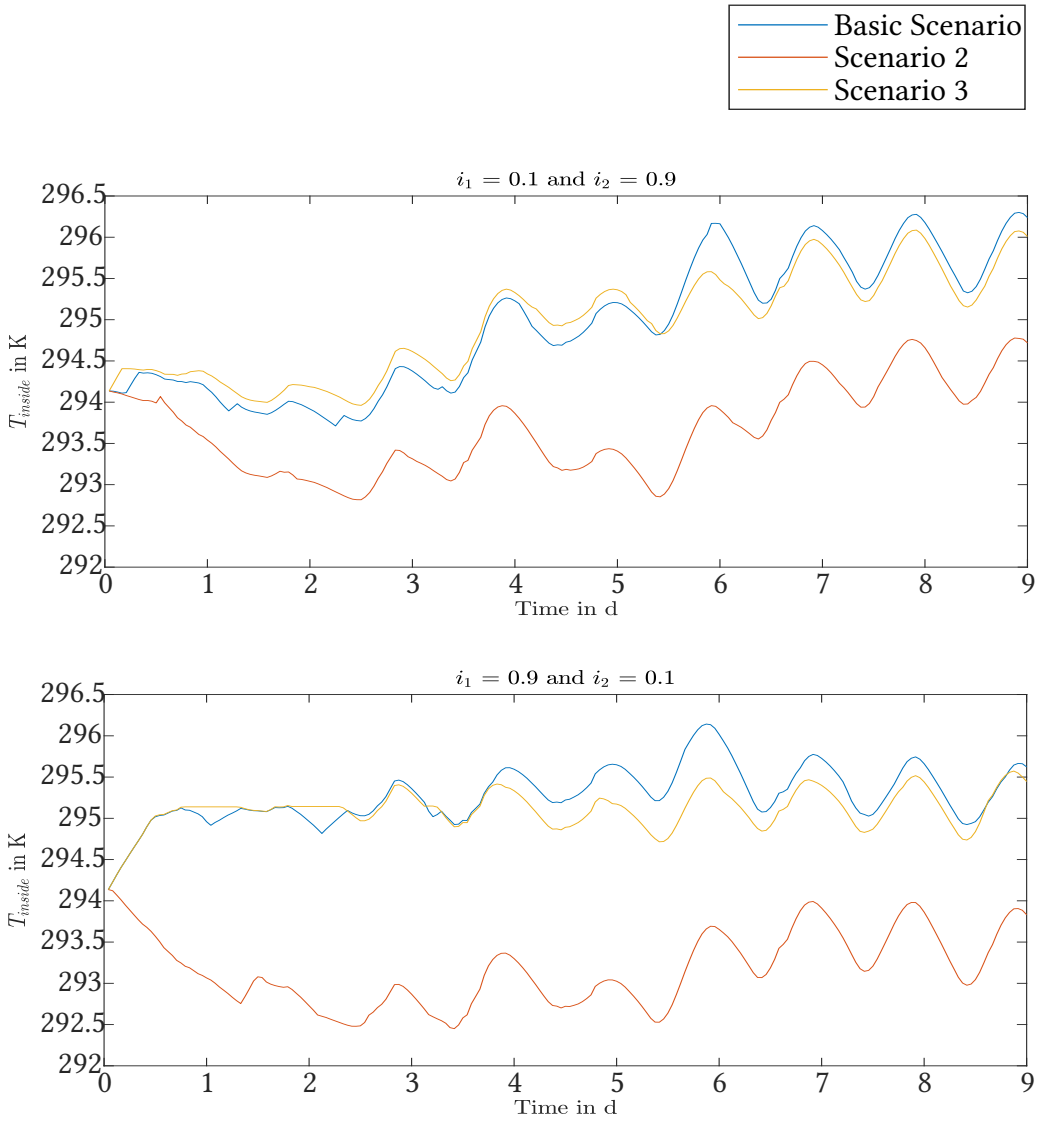

Figure 6.1. T_{inside} for the three scenarios for $i_1 = 0.1 and i_2 = 0.9$ and $i_1 = 0.9 and i_2 = 0.1$

In Figure 6.2, $\dot{Q}_{\text{heating}}$ is depicted over the simulation period. Also, the weightings are distinguished in two diagrams. We see negative and positive values for $\dot{Q}_{\text{heating}}$ in all scenarios and further some constant values.

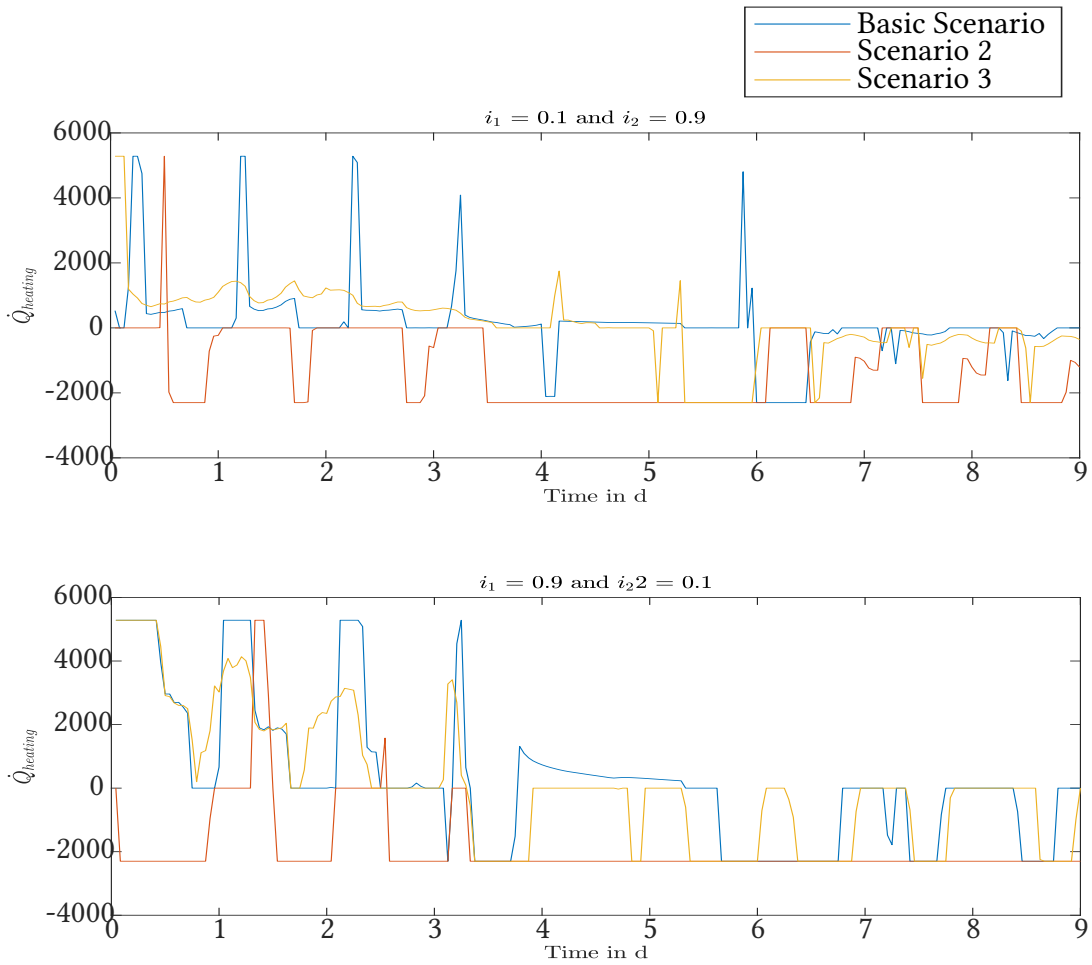

Figure 6.2. $\dot{Q}_{\text{heating}}$ for the three scenarios for $i_1 = 0.1 and i_2 = 0.9$ and $i_1 = 0.9 and i_2 = 0.1$

Figure 6.3 illustrates the heat flow $\dot{Q}_{\text{HP}}$ for all scenarios over the simulation time with both weightings. We notice that scenario 2 differs stronger of the other scenarios and the basic scenario has a constant period during from day three to five. The values are in both diagrams positive and negative and we see higher absolute values in the second diagram with $i_1 = 0.9 and i_2 = 0.1$.

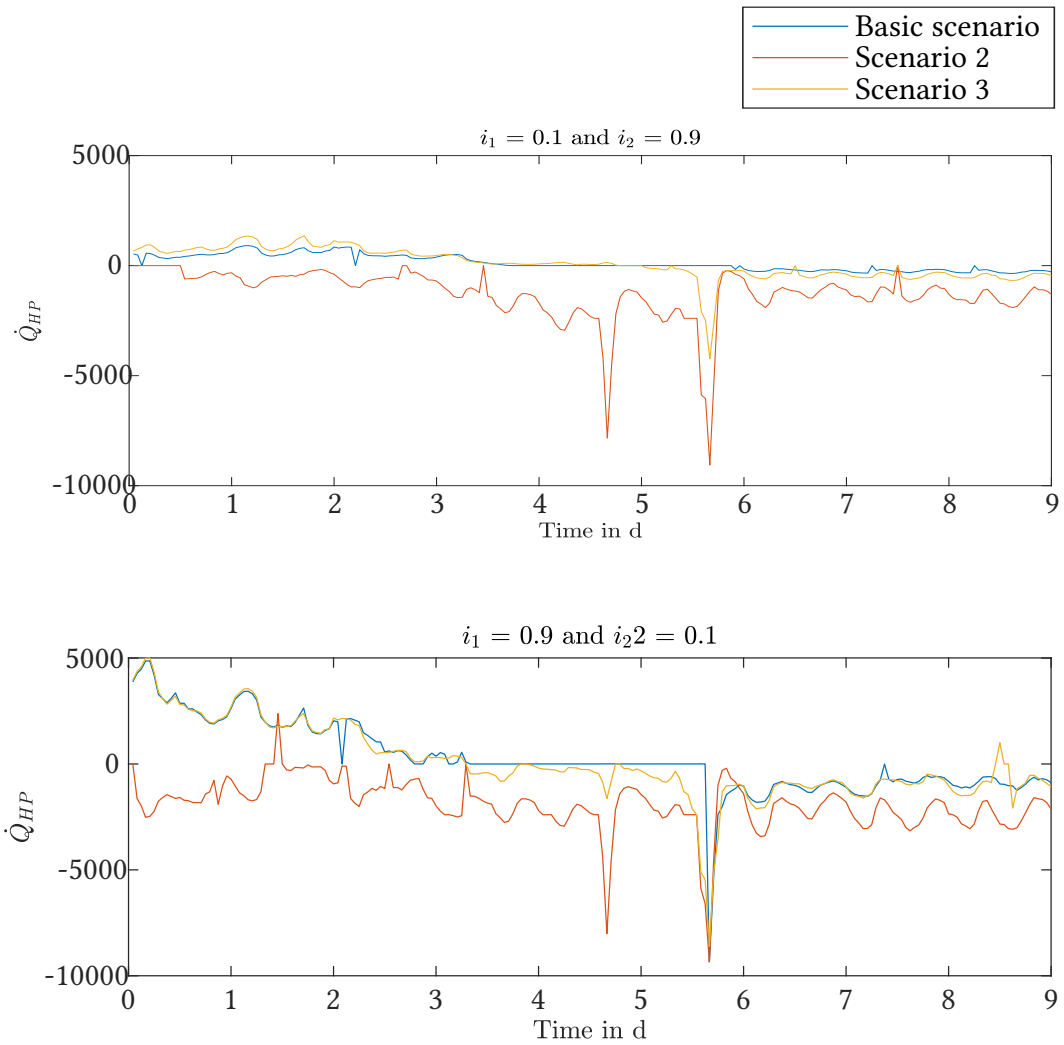

Figure 6.3. $\dot{Q}_{\mathrm{HP}}$ for the three scenarios for $i_1 = 0.1 and i_2 = 0.9$ and $i_1 = 0.9 and i_2 = 0.1$

In the following Figure 6.4 the structure for the comparison between the scenarios differs from the Figures above. Here, we separate every scenario in its diagram and vary the weightings within the diagram. The first diagram shows the curve of the electricity consumption of the heat pump for the basic scenario with $i_1 = 0.1 and i_2 = 0.9$ and $i_1 = 0.9 and i_2 = 0.1$ during the simulation period. Further, the dynamic electricity price Pr is illustrated at the same time. Both further diagrams depict the same for the other scenarios. Pr is independent of the scenarios. Therefore, we see three times the same curves in every diagram. The curves of P_{HP} with the lower weighting on grid services run above those with higher weighting on grid services. Further, some yellow highlights are at the x-axis, which is needed for a better discussion below.

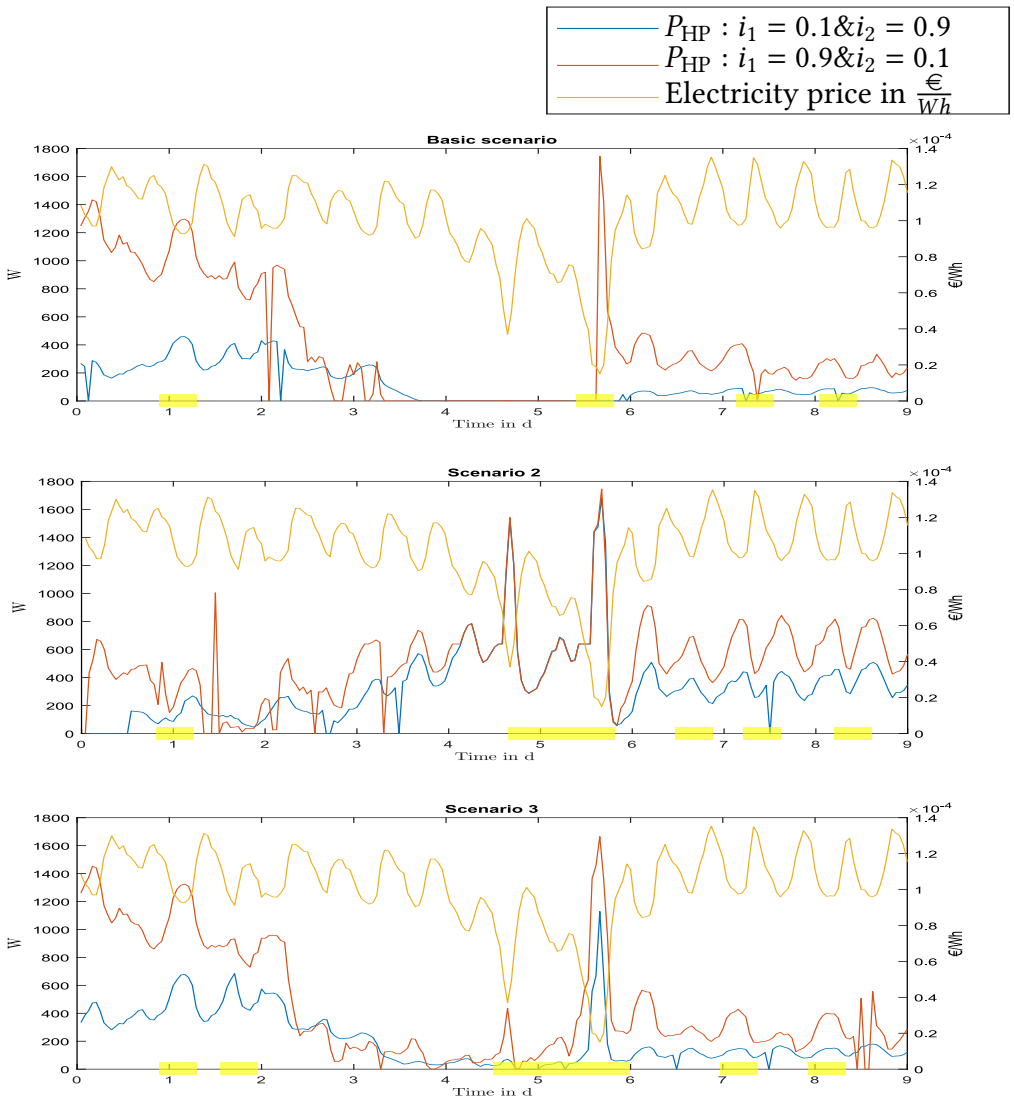

Figure 6.4. P_{HP} and Pr for the three scenarios for $i_1 = 0.1 and i_2 = 0.9$ and $i_1 = 0.9 and i_2 = 0.1$

Table 6.1 presents the average comfort $\Delta\overline{y}$ of the scenarios calculated according to Equation 5.7. We also differentiate the weighting of comfort with $i_1 = 0.1$ or 0.9. Scenario 2 has the highest values of $\Delta\overline{y}$ and the basic scenario and scenario 3 changes the order with the weighting. Only scenario 2 has a high $\Delta\overline{y}$ with higher weighting of comfort.

i_1	Basic scenario	Scenario 2	Scenario 3
0.1	0.77	1.46	0.55
0.9	0.13	2.02	0.17

Table 6.1. $\Delta\overline{y}$ of the scenarios according to i_1

Table 6.2 shows the equivalent of the table above but grid services (GS) is of interest, also with two weightings $i_2 = 0.1$ or 0.9. The values of GS are presented for every scenario calculated according to Equation 5.8. The lower values of GS depend on higher weighting of grid services.

i_2	Basic scenario	Scenario 2	Scenario 3
0.1	9.00	10.40	9.69
0.9	2.85	6.36	4.57

Table 6.2. GS of the scenarios according to i_2

Table 6.3 depicts the energy consumption in kWh as the sum of the power of P_{HP} over the simulation period. We separate the weighting consideration of every scenario. All scenarios have higher energy consumption with higher weighting on the comfort requirement in the cost function. The basic scenario has the lowest values.

i_1 & i_2	Basic scenario	Scenario 2	Scenario 3
0.1 & 0.9	5,699 kWh	15,572 kWh	9,866 kWh
0.9 & 0.1	18,533 kWh	23,666 kWh	21,015 kWh

Table 6.3. Energy consumption of the scenarios according to the weighting

6.2. Discussion

The presented results from subsection 6.1.2 are explained and analysed in this section. In addition, the general realisation of this thesis is discussed.

6.2.1. Comparison of the scenarios

To compare the different scenarios, we use the results in the section above. We comment every Figure and Table from subsection 6.1.2.
We observe in the inside temperature curves from Figure 6.1 that the desired temperature y_{track} of the scenarios cannot be reached. For better analysing, we consider Figure 6.2 with the control signal $\dot{Q}_{heating}$. The heat flow $\dot{Q}_{heating}$ often runs in constant maximum or minimum, which means a reaching of the limits of the constraints. Although the absolute control signal is maximum, we have deviations from y_{track}. This behaviour indicates that the thermal model reacts not strong enough on the given control signals.
Obviously, T_{inside} of scenario 2 runs below the other scenarios. The reason for that follows from the changing desired temperature between 290.15 K and 295.15 K. Since in scenario 2, the comfort requirement in the cost function during the presence and the absence of occupants is weighted the same, the optimiser does not differentiate between these two cases and generates the best for both. It follows the inferior performance of the average comfort in Table 6.1 compared to the other scenarios. Especially is the effect that a higher weighting on comfort in the cost function results in a higher $\Delta\overline{y}$. By way of explanation, we first note that the absence phase of occupants is longer than the presence phase of occupants, which is predominantly due to the weekend work break. Focusing the comfort requirement in the cost function of scenario 2, the deviation of T_{inside} from the desired temperature during absence $y_{\text{track,absence}}$ is lower due to the longer phase. This increases the difference between the actual temperature and the desired temperature during the presence phase, which the control signal cannot compensate. Consequently, we obtain a poorer average comfort with a higher weighting of the comfort requirement in scenario 2 (see Table 6.1).
T_{inside} of the basic scenario and scenario 3 run close together, with scenario 3 always closer to $y_{\text{track}} = 295.15K$ (Figure 6.1). A constant desired temperature over the whole day affects consequently positive on the comfort. We note this further for the $\Delta\overline{y}$ with the lower weighting i_1 in Table 6.1. Also, in Figure 6.1 and Table 6.1 it is visible that a higher weighting on the comfort effects the expected improvement of the comfort. We notice a slightly better $\Delta\overline{y}$ of the basic scenario of 0.04 K than scenario 3 with i_2. This results form the calculation of $\Delta\overline{y}$ wherein only the presence of occupants is considered. Due to the consideration of scenario 3 without an occupancy schedule, it is assumed that occupants are always in the building and that comfort must always be maintained. Thus, we sum more temperature deviations for obtaining $\Delta\overline{y}$ of scenario 3 and divide by a higher number of n_{occ}. Nevertheless, this results in

a slight decline of $\Delta\overline{y}$ compared to the basic scenario with the weighting $i_1 = 0.9$.
Figure 6.2 and Figure 6.3 depict the optimised control signals. We note that the optimiser avoids different signs of $\dot{Q}_{\mathrm{HP}}$ and $\dot{Q}_{\mathrm{heating}}$ so that the water reservoir and the building is heated or cooled, as it is constrained. Further, we observe a constant phase of $\dot{Q}_{\mathrm{HP}}$ between the fourth and the sixth day of the basic scenario in Figure 6.3. These days fall on the weekend, which means a longer phase without the comfort requirement in the cost function of the basic scenario. The phase exceeds the length of the predictive horizon, wherefore no energy has to be stored at favorable times according the forecasting calculations. Therefore, the optimiser chooses $\dot{Q}_{\mathrm{HP}} = 0$ to enable zero cost in the cost functions.
The electrical consumption of the heat pump P_{HP} is more interesting than $\dot{Q}_{\mathrm{HP}}$ because P_{HP} influences directly the grid, which is investigated. However, P_{HP} is calculated from $\dot{Q}_{\mathrm{HP}}$ (see subsection 5.1.1).
Figure 6.4 and Table 6.2 provide clarification about the grid services of the scenarios. In both representations, it is obviously that a higher weighting on grid services requirement in the cost function leads to lower values of $\dot{Q}_{\mathrm{HP}}$ (see Figure 6.3) and consequently of P_{HP} (see Figure 6.4). Since the higher weighting i_2 would lead to higher cost with higher values for $\dot{Q}_{\mathrm{HP}}$.
To determine which scenario is more suitable for grid services, we examine the amplitudes of P_{HP} at cheap or expensive electricity prices Pr. The yellow highlights in Figure 6.4 mark obvious spots where the heat pump reacts as desired: at low prices Pr, which indicate a higher available load on the grid, the heat pump reacts with a larger control signal and at higher Pr, with a lower control signal. In general, all scenarios behave according to the specifications of the grid. Because the basic scenario does not consume power at the weekend, it does not react to the grid for a longer time and can therefore be classified with less grid service than the other two scenarios. It also requires the least costs for the entire period of the simulation, as revealed by Table 6.2, while scenario 2 requires the most costs. Scenario 2 reacts with the high amplitudes the strongest on the Pr. Therefore, it is the best scenario for grid services. Scenario 2 is only interesting because of the investigation of grid services. Focusing on the energy consumption, scenario 2 waste energy (see the most high energy consumption in Table 6.3). The basic scenario, with the occupancy schedule, requires at least energy.

We can summarise the comparing of the scenarios and analysis of the results. Even if the thermal model does not react not as well as desired, nevertheless, the research question is answerable. The inclusion of an occupancy schedule in the MPC improves the energy consumption if we proceed as the basic scenario. The opposite to the basic scenario is scenario

3. More grid services can be reached with a time-independent cost function as scenario 2 or 3, where both requirements grid services and comfort always are of interest. Scenario 2 reacts most on grid services and scenario 3 most on comfort. Nevertheless, considering the energy consumption, neither of the two scenarios can be recommended. The basic scenario enables the compromise on energy consumption and grid services. At the same time, a higher weighting of comfort in relation to grid services can be recommended. This will give us more influence on the grid while increasing comfort.

6.2.2. General discussion about the approach

In this subsection, we comment further issues affecting all scenarios to give an analysis over the used approach and clarify the limitations.

feasible problem

During the implementation of the MPC, es hat sich herausgestellt, dass einfache veränderungen im Code schnell zu unlösbaren problemen führt. Das Modell, die constraints und die Gewichte der Kostenfunktion haben hier großen einfluss auf das finden einer lösung.

cooling and heating

The approach enables cooling and heating of the reference building. Damit kann mit einem modell winter und sommer abgedeckt werden. Jedoch muss das Modell winter und sommer ausreichend gut modellieren. Das in diesem Ansatz gewählte modell wurde nur für den Sommer verifiziert. Durch das erlauben von kühlen und heizen gewinnt der optimierer mehr freiheitsgrade, wodurch ein nutzverhalten entsteht wie es bei einem manuellen anwender nicht vorkommen würde. es wird innerhalb eines Tages geheizt und gekühlt.

7. Conclusion

8. Outlook

Bibliography

[1] United Nations. *Paris Agreement*. 2015.

[2] Deutschlandfunk, ed. *Auf dem Weg zur Klimaneutralität: Die neuen Klimaziele für Deutschland*. 24.06.2021.

[3] Bundesregierung. *Abschied von der Kohleverstromung: Fragen und Antworten*. Ed. by Presse- und Informationsamt der Bundesregierung. 2021.

[4] C. W. Gellings. *The concept of demand-side management for electric utilities*. In: *Proceedings of the IEEE*, Vol. 73, No. 10 (1985), pp. 1468–1470.

[5] P. Kohlhepp and V. Hagenmeyer. *Technical Potential of Buildings in Germany as Flexible Power-to-Heat Storage for Smart-Grid Operation*. In: *Energy Technology*, Vol. 5, No. 7 (2017), pp. 1084–1104.

[6] Karl-Heinz Backhaus (Vaillant), Dr. Hendrik Ehrhardt (Stiebel Eltron), André Jacob (BWP), Barbara. *Branchenstudie 2021: Marktanalyse - Szenarien - Handlungsempfehlungen: Vorabveröffentlichung zum*. In: (24.11.2020).

[7] F. Oldewurtel, A. Ulbig, A. Parisio, G. Andersson, and M. Morari. *Reducing peak electricity demand in building climate control using real-time pricing and model predictive control*. In: (2010), pp. 1927–1932.

[8] I. Hazyuk, C. Ghiaus, and D. Penhouet. *Optimal temperature control of intermittently heated buildings using Model Predictive Control: Part II – Control algorithm*. In: *Building and Environment*, Vol. 51 (2012), pp. 388–394.

[9] P. Zwickel, A. Engelmann, L. Groll, V. Hagenmeyer, D. Sauer, and T. Faulwasser. *A Comparison of Economic MPC Formulations for Thermal Building Control*. In: *2019 IEEE PES Innovative Smart Grid Technologies Europe (ISGT-Europe)*. IEEE, 29.09.2019 - 02.10.2019, pp. 1–5.

[10] W. Wang, J. Zhang, B. Michael, and B. Futrell. *Energy Savings of Occupancy-Based Controls in Office Buildings*. In: (2019), pp. 932–939.

[11] R. Kramer, J. van Schijndel, and H. Schellen. *Simplified thermal and hygric building models: A literature review*. In: *Frontiers of Architectural Research*, Vol. 1, No. 4 (2012), pp. 318–325.

[12] H. Harb, N. Boyanov, L. Hernandez, R. Streblow, and D. Müller. *Development and validation of grey-box models for forecasting the thermal response of occupied buildings*. In: *Energy and Buildings*, Vol. 117, No. 6 (2016), pp. 199–207.

[13] S. Freund and G. Schmitz. *Entwicklung und Validierung von Grey-Box-Modellen zur Modellierung des thermischen Verhaltens von Einzelbüros in einem Niedrigenergie-Bürogebäude*. In: (2020).

[14] Evelyn Sperber. *Grey-Box-Modellierung des thermischen Verhaltens von Typgebäuden*. 11. Internationale Energiewirtschaftstagung. 2019.

[15] D. Coakley, P. Raftery, and M. Keane. *A review of methods to match building energy simulation models to measured data*. In: *Renewable and Sustainable Energy Reviews*, Vol. 37 (2014), pp. 123–141.

[16] Jiří Cigler, Jaň Sirok, Milan Korda, and Colin N Jones. *On the Selection of the Most Appropriate MPC Problem Formulation for Buildings*. In: (2013).

[17] Danny Günther, Jeannette Wapler, Robert Langner, Sebastian Helmling, Dr.-Ing. Marek Miara, Dr.-Ing. David Fischer, Dirk Zimmermann, Tobias Wolf, Dr.-Ing. Bernhard Wille-Hausmann. *Wärmepumpen in Bestandsgebäuden: Ergebnisse aus dem Forschungsprojekt "WPsmart im Bestand": Abschlussbericht*. Ed. by Fraunhofer Institut für Solare Energiesysteme ISE. Freiburg, 2020.

[18] M. Avci, M. Erkoc, A. Rahmani, and S. Asfour. *Model predictive HVAC load control in buildings using real-time electricity pricing*. In: *Energy and Buildings*, Vol. 60 (2013), pp. 199–209.

[19] G. Bianchini, M. Casini, D. Pepe, A. Vicino, and G. G. Zanvettor. *An integrated model predictive control approach for optimal HVAC and energy storage operation in large-scale buildings*. In: *Applied Energy*, Vol. 240, No. 1 (2019), pp. 327–340.

[20] D. Kim and J. E. Braun. *Hierarchical Model Predictive Control Approach for Optimal Demand Response for Small/Medium-sized Commercial Buildings*. In: (2018), pp. 5393–5398.

[21] G. Bianchini, M. Casini, A. Vicino, and D. Zarrilli. *Demand-response in building heating systems: A Model Predictive Control approach*. In: *Applied Energy*, Vol. 168, No. 3 (2016), pp. 159–170.

[22] X. Liang, T. Hong, and G. Q. Shen. *Occupancy data analytics and prediction: A case study*. In: *Building and Environment*, Vol. 102 (2016), pp. 179–192.

[23] H. D. Baehr and S. Kabelac, eds. *Thermodynamik*. Berlin, Heidelberg: Springer Berlin Heidelberg, 2016.

[24] *VDI-Wärmeatlas*. Berlin, Heidelberg: Springer Berlin Heidelberg, 2013.

[25] H. Kuchling, ed. *Taschenbuch der Physik: Mit zahlreichen Tabellen*. 19., aktualisierte Aufl. München: Fachbuchverl. Leipzig im Carl-Hanser-Verl., 2007.

[26] A. Griesinger, ed. *Wärmemanagement in der Elektronik*. Berlin, Heidelberg: Springer Berlin Heidelberg, 2019.

[27] H. D. Baehr and K. Stephan, eds. *Wärme- und Stoffübertragung*. Berlin, Heidelberg: Springer Berlin Heidelberg, 2016.

[28] I. Hazyuk, C. Ghiaus, and D. Penhouet. *Optimal temperature control of intermittently heated buildings using Model Predictive Control: Part I – Building modeling*. In: *Building and Environment*, Vol. 51 (2012), pp. 379–387.

[29] L. Grüne and J. Pannek. *Nonlinear model predictive control: Theory and algorithms*. Second edition. Communications and control engineering. Cham: Springer, 2017.

[30] J. T. Wen and S. Mishra, eds. *Intelligent Building Control Systems: A Survey of Modern Building Control and Sensing Strategies*. Advances in Industrial Control. Cham: Springer, 2018.

[31] F. Oldewurtel, A. Parisio, C. N. Jones, D. Gyalistras, M. Gwerder, V. Stauch, B. Lehmann, and M. Morari. *Use of model predictive control and weather forecasts for energy efficient building climate control*. In: *Energy and Buildings*, Vol. 45, No. 9 (2012), pp. 15–27.

[32] B. Kouvaritakis and M. Cannon, eds. *Model Predictive Control*. Cham: Springer International Publishing, 2016.

[33] J. Široký, F. Oldewurtel, J. Cigler, and S. Prívara. *Experimental analysis of model predictive control for an energy efficient building heating system*. In: *Applied Energy*, Vol. 88, No. 9 (2011), pp. 3079–3087.

[34] Karlsruher Institut für Technologie. *Energy Lab 2.0*. https://www.elab2.kit.edu/index.php, 15.07.2021.

[35] Bundesverband Wärmepumpe e.V. *Positives Signal für den Klimaschutz: 40 Prozent Wachstum bei Wärmepumpen*. 19.01.2021.

[36] ratiotherm Smart Energy Systems, ed. *Technische Daten: Oskar°Wärmepumenspeicher WPS*.

[37] Udo Machauer. *Bauplan_Wärmepumpenhaus*. Ed. by Karlsruher Institut für Technologie. 2017.

[38] Statusseminar. Forschung für Energieoptimiertes Bauen, ed. *Modellbasierte Betriebsanalyse von Gebäuden - Methoden für die Fehlererkennung und Optimierung im Gebäudebetrieb*. 2009.

[39] S. Estrada-Flores, I. Merts, B. DE Ketelaere, and J. Lammertyn. *Development and validation of "grey-box" models for refrigeration applications: A review of key concepts*. In: *International Journal of Refrigeration*, Vol. 29, No. 6 (2006), pp. 931–946.

[40] IDM ENERGIESYSTEME GMBH. *Technische Unterlagen Montageanleitung: AERO SLM 3- 11 AERO SLM 6- 17: Zusätzliche Ausstattungsvarianten HGL ohne HGL*.

[41] H. Park, M. Ruellan, A. Bouvet, E. Monmasson, and R. Bennacer. *Thermal parameter identification of simplified building model with electric appliance*. In: *11th International Conference on Electrical Power Quality and Utilisation (EPQU), 2011*. Piscataway, NJ: IEEE, 2011, pp. 1–6.

[42] B. Weigand, J. Köhler, and J. VON Wolfersdorf, eds. *Thermodynamik kompakt – Formeln und Aufgaben*. Berlin, Heidelberg: Springer Berlin Heidelberg, 2016.

[43] Anton Schweizer. *Formelsammlung und Berechnungsprogramme Maschinen- und Anlagenbau: Wärmeübergangskoeffizienten - Gase - Luft -*. Ed. by Schweizer-fn.

[44] Thorben Frahm. *Ein Fenster mit niedrigem U-Wert spart Energie*. Ed. by D. UND Sanieren. 2021.

[45] Anton Schweizer. *Formelsammlung und Berechnungsprogramme Maschinen- und Anlagenbau: Wärmeleitfähigkeit verschiedener Matereialien*. Ed. by Schweizer-fn. 12.10.2021.

[46] K. Ghazi Wakili, E. Hugi, L. Karvonen, P. Schnewlin, and F. Winnefeld. *Thermal behaviour of autoclaved aerated concrete exposed to fire*. In: *Cement and Concrete Composites*, Vol. 62, No. 283 (2015), pp. 52–58.

[47] Abteilung Klima- und Umweltberatung. *Jahresmittel der Windgeschwindigkeit - 10 m über Grund - in Baden-Württemberg: Statistisches Windfeldmodell (SWM).* Offenbach, 2004.

[48] Anton Schweizer. *Formelsammlung und Berechnungsprogramme Maschinen- und Anlagenbau: Wärmekapazität verschiedener Materialien.* Ed. by Schweizer-fn. 12.10.2021.

[49] A. G. Barnston. *Correspondence among the Correlation, RMSE, and Heidke Forecast Verification Measures; Refinement of the Heidke Score.* In: *Weather and Forecasting*, Vol. 7, No. 4 (1992), pp. 699–709.

[50] Thermoval Polska. *Konwektor elektryczny TX 2000, 2,0 kW, IP20, biały: Kod produktu: 5 901 812 594 495.*

[51] Fakir-Hausgeräte GmbH. *prestige | HK 2010CT: Bedienungsanleitung Konvektor.* 2016.

[52] Trotec GmbH. *TDS 10 / TDS 20 / TDS 30 / TDS 50: Originalbetriebsanleitung Elektroheizer.*

[53] Bundesnetzagentur | SMARD.de. Ed. by Bundesnetzagentur für Elektrizität, Gas, Telekommunikation, Post und Eisenbahnen. www.smard.de.

[54] Andreas Kejzlar. *Roth Flächentemperierung: Roth_Auslegung_Fbh.* Ed. by Roth Energiesysteme Sanitärsysteme. 21.01.2020.

[55] SEF Ingenieurgesellschaft MBH. *KÜHLLASTBERECHNUNG VDI 2078.* 5.09.2019.

[56] Umweltbundesamt. *Richtig heizen: Richtige Raumtemperatur finden.* Ed. by Bundesrepublik Deutschland. 7.10.2021.

[57] Bund. *Technische Regeln für Arbeitsstätten Raumtemperatur (ASR A3.5): 4.2 Lufttemperaturen in Räumen.* 2021.

[58] J. Drgoňa, J. Arroyo, I. Cupeiro Figueroa, D. Blum, K. Arendt, D. Kim, E. P. Ollé, J. Oravec, M. Wetter, D. L. Vrabie, and L. Helsen. *All you need to know about model predictive control for buildings.* In: *Annual Reviews in Control*, Vol. 50, No. 16 (2020), pp. 190–232.

[59] Kai Furmans, Marcus Geimer, Balazs Pritz, Carsten Proppe, ed. *Skriptum zur Vorlesung: Modellbildung und Simulation.* WS19/20.

[60] Joel A. E. Andersson, Joris Gillis, Greg Horn, James B. Rawlings, and Moritz Diehl. *CasADi – A software framework for nonlinear optimization and optimal control.* In: (2018).

Nomenclature

Acronyms

DSM	Demand Side Management
GS	Costs for grid services
HoHe	Household Heater without a fan
HoHeF	Household Heater with a Fan
HP	Heat Pump
HVAC	Heating, Ventilation, and Air Conditioning
IH	Indusrial Heater
KIT	Karlsruhe Institute of Technology
MPC	Model Predictive Control
PLC	Programmable Logic Controller
RMSE	Root Mean Square Error
SW	Service Water
UN	United Nations
WR	Water Reservoir

Greek letters

α	heat transfer coefficient	$W/(m^2K)$
λ	thermal conductivity	$W/(mK)$

Physical size

$\Delta\overline{y}$	Average comfort	
ΔT	temperature difference	K
$\partial T/\partial x$	temperature gradient	K/m
U	inner energy	J
N	length of the predictive horizon	
Pr	dynamic Price of the electricity	

A. Appendix

A.1. Model values

	Start values	Identified values
C_{inside}	400425 J/W	1198069 J/W
C_{envelope}	24999045 J/W	24998057 J/W
C_{interior}	22960754 J/W	22960750 J/W
C_{floor}	26118734 J/W	26118731 J/W
R_{inside}	191 K/W	0,66 K/W
R_{window}	34 K/W	0.0025 K/W
R_{envelope}	287 K/W	0,00008 K/W
R_{interior}	77 K/W	28001 K/W
R_{floor}	749 K/W	2719 K/W
R_{in}	191 K/W	191 K/W
$f_{\text{sol,inside}}$	0,25	7.80685 K/W
$f_{\text{sol,envelope}}$	0,25	-7.30632 K/W

Table A.1. Start and identified values of the model parameters

A.2. Matrices of state-space formulation

$$B_1 = \begin{pmatrix} 1 & 0 \\ 0 & 0 \\ 0 & 0 \\ 0 & 0 \\ -1 & 1 \end{pmatrix} \tag{A.1}$$

$$B_2 \begin{pmatrix} f_{sun,inside} & 0 & \frac{1}{C_{inside}R_{window}} & 0 \\ 0 & f_{sun,envelope} & \frac{1}{C_{envelope}R_{envelope}} & 0 \\ 0 & 0 & 0 & 0 \\ 0 & 0 & 0 & 0 \\ 0 & 0 & 0 & -1 \end{pmatrix} \tag{A.2}$$

$$C = \begin{pmatrix} 1 & 0 & 0 & 0 & 0 \end{pmatrix} \tag{A.3}$$

$$
A = \begin{pmatrix}
\frac{-1}{C_{inside}R_{inside}} - \frac{1}{C_{inside}R_{window}} - \frac{1}{C_{inside}R_{interior}} - \frac{1}{C_{inside}R_{floor}} & \frac{1}{C_{inside}R_{inside}} & \frac{1}{C_{inside}R_{interior}} & \frac{1}{C_{inside}R_{floor}} \\
\frac{1}{C_{envelope}R_{inside}} & \frac{-1}{C_{envelope}R_{envelope}} - \frac{1}{C_{envelope}R_{inside}} & 0 & 0 \\
\frac{1}{C_{interior}R_{interior}} & 0 & -\frac{1}{C_{interior}R_{interior}} & 0 \\
\frac{1}{C_{floor}R_{floor}} & 0 & 0 & -\frac{1}{C_{floor}R_{floor}} \\
0 & 0 & 0 & 0
\end{pmatrix} \tag{A.4}
$$

A.3. Laboratory journal

Experiment: 16. July - 18. July 2021

Time	Location	Incident
16.7.21 9.30pm	Room 1	HoHe on
	Room 2	HoHeF on
	Floor 2	IH on
		closed doors
18.7.21 0.00am	Room 2	HoHeF off
		rearrange HoHeF
	Kitchen	HoHeF on
18.7.21 9.30pm	Room 1	HoHe off
	Kitchen	HoHeF off
	Floor 2	IH off
		opened doors and windows

Table A.2. Laboratory journal: 16. July - 18. July 2021

Experiment: 16. July - 18. July 2021

Time	Location	Incident
26.7. - 27.7.21	Kitchen	HoHeF on
10.00pm - 5.00am		closed door
27.7. - 28.7.21	Kitchen	HoHeF on
10.00pm - 4.00am		closed door
28.7. - 29.7.21	Kitchen	HoHeF on
10.00pm - 5.00am		opened door
5.00am - 8.20am		closed door
29.7. - 30.7.21	all	breakdown PLC
16.00pm - 9.30am	Kitchen	HoHeF still off
30.7.21 9.30pm	Room 1	HoHe on
	Room 2	HoHeF on
	Floor 2	IH on
		opened doors
31.7. - 1.8.21	all	breakdown PLC
2.30pm - 9.20am		
31.7.21 4.00pm	Room 1	HoHe off
	Room 2	HoHeF off
7.30pm	Floor 2	IH off
	Room 2	rearrange HoHeF
1.8.21 9.30pm	Room 1	HoHe on
	Kitchen	HoHeF on
		PLC works
1.8.21	all	breakdown PLC
11.30am - 0.20pm		
1.8.21 9.30pm	Room 1	HoHe off
	Kitchen	HoHeF off
	Floor 2	IH off
		opened doors and windows

Table A.3. Laboratory journal: 26. July - 1. August 2021

A.4. Average comfort and grid services

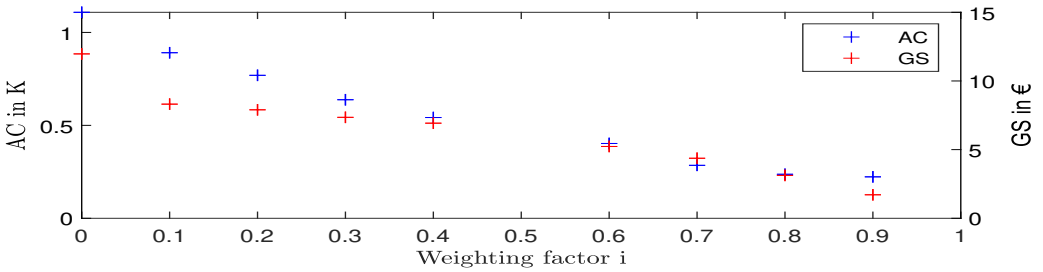

Figure A.1. AC and GS for N = 12h

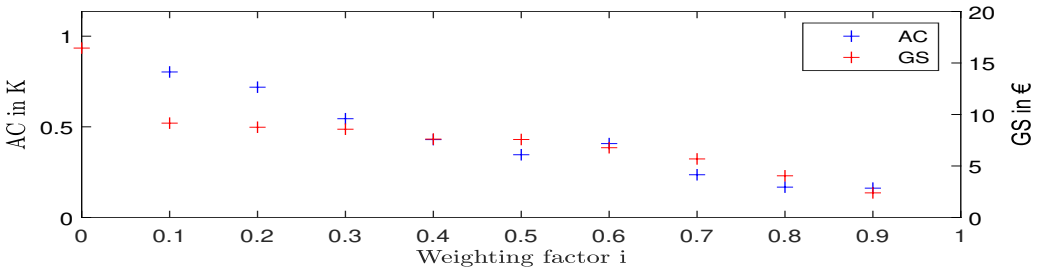

Figure A.2. AC and GS for N = 18h

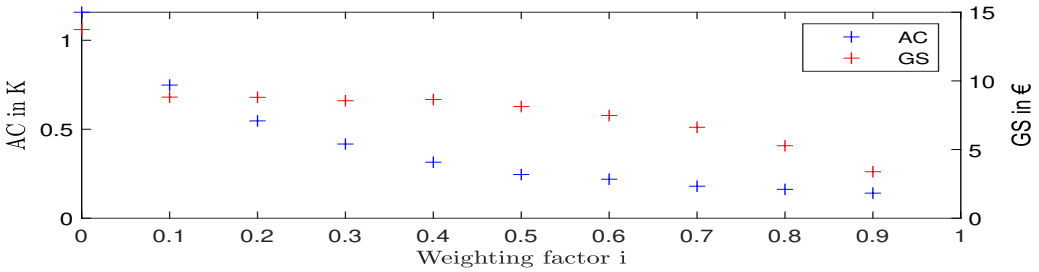

Figure A.3. AC and GS for N = 30h

...